

Preparation and characterization of the
Protein A-immobilized PVDF and PES
microporous membranes activated by the
atmospheric pressure low temperature
plasma

The doctoral dissertation

September 2014

Naohisa Akashi

Supervisor: Professor Shin-ichi Kuroda

Department of production science and technology

Graduate school of engineering

Gunma University

Contents

Chapter 1	4
1.1 General introduction	4
1.2 Microporous membranes.....	8
1.3 Plasma	12
1.4 Affinity membranes.....	18
1.5 Objectives and originalities of this study	19
References	23
Chapter 2 Protein immobilization onto polyvinylidene fluoride microporous membranes activated by the atmospheric pressure low temperature plasma.....	26
2.1 Introduction	26
2.2 Experimental	28
2.2.1 Materials	28
2.2.2 Plasma reactor and plasma treatments.....	28
2.2.3 Immobilization procedure	30
2.2.4 Physical and chemical surface characterization	31
2.2.5 Membrane morphology	33
2.3 Results and discussion	34
2.3.1 Hydrophilicity characterization	36
2.3.2 Dependence of the degree of grafting on reaction conditions.....	39
2.3.3 Structure characterization of the membranes by ATR-FTIR analysis	42
2.3.4 Structure characterization of the membranes by XPS analysis	45
2.3.5 The activation mechanism for initiation of graft polymerization.....	58
2.3.6 Dependence of the degree of BSA conjugation on reaction conditions	63
2.3.7 Membrane morphology	68
2.4 Conclusions.....	75
References.....	76
Chapter 3 Preparation and characterization of Protein A-immobilized PVDF and PES membranes.....	80
3.1 Introduction.....	80
3.2 Experimental	83
3.2.1 Materials	83
3.2.2 Preparation of the PVDF and PES membranes immobilized with Protein A..	83

3.2.3 Physical and chemical surface characterization	86
3.2.4 Determination of adsorption capacities	86
3.2.5 Determination of ligand densities.....	88
3.2.6 Procedure of stability test	88
3.3 Results and discussion	89
3.3.1 Structure characterization of the membranes by ATR-FTIR analysis	89
3.3.2 Structure characterization of the membranes by XPS analysis	92
3.3.3 Determination of the human IgG adsorption capacity of affinity membranes.....	105
3.3.4 Membrane morphology	114
3.4 Conclusions	116
Nomenclature	117
References	118
Chapter 4 Summary	122
List of publications	124
Acknowledgements	125

Chapter 1

1.1 General introduction

The necessity of biologicals has been increasing in clinical field. As one of the reasons, biologicals are effective at the diseases which could not treat or relieve with conventional pharmaceutical products because of the high specificity against each target. The biologicals are used for diseases such as cancers, diabetes and rare illnesses, and bring profits to patients more than 350 million all over the world [1]. Biologicals have various types such as protein medicines, nucleic acid medicines, peptide medicines and antibody drugs, etc [2]. In these, antibody drugs are used for the treatment such as breast cancer, B-cell lymphoma, and rheumatoid arthritis. The majority of the approved antibodies are targeting cancer and autoimmune diseases with the top 5 grossing antibodies populating these two areas. In addition, over 100 monoclonal antibodies (mAbs) are in Phase II and III of clinical development, and numerous others are in various pre-clinical and safety studies [3]. However, there are issues that the production cost is higher than those of low molecule drugs, because large-scale facilities for the commercial production are necessary at approximately more than 1,000 L, and raw materials, facility and utility maintenances are expensive generally. As an example indicated systematically, Fig. 1.1 shows the steps in a production process for drug substance. The production processes mainly consist of cell culture steps and purification steps.

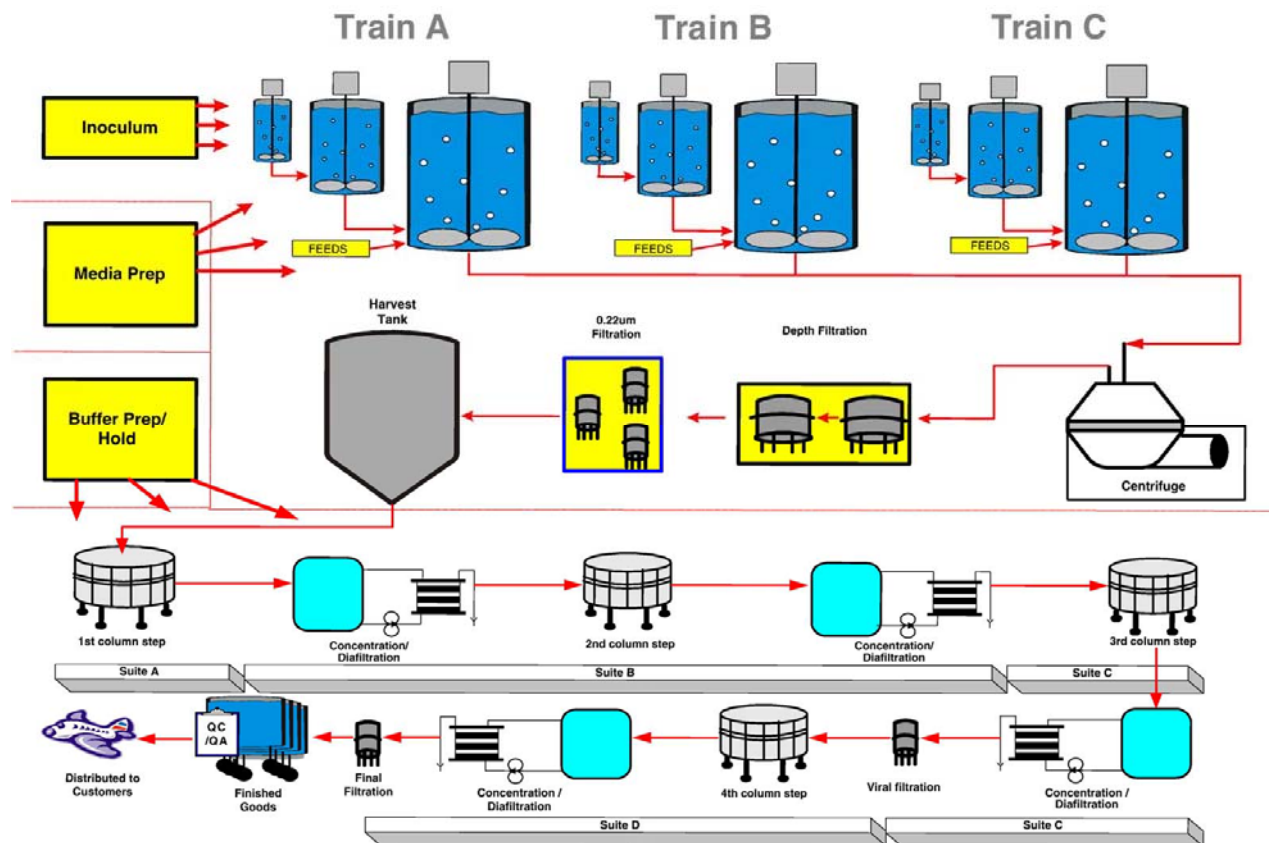


Fig. 1.1. Process flow for a large-scale facility for manufacturing proteins [4].

First of all, culture process starts thawing working cell bank, and cells are expanded through small reactors into inoculum vessels in the production train. At the end of the culture, the supernatant of the reactor are harvested by a centrifugation and through filters prior to purification in a series of chromatography steps. The purification steps generally consist of three steps, that is, capture, intermediate purification and polishing steps. In the first chromatography step of mAbs production, the Protein A chromatography is adopted predominantly as the capture step, because the production yield of the affinity mode is higher relative to the other mode. Although Protein A chromatography media can be used repeatedly, the purchase price overwhelms the cost of other materials for the production. The next process of the affinity chromatography often employs the viral inactivation due to the low pH. According to the good manufacturing practice guide for active pharmaceutical ingredients Q7, it is described that viral inactivation and viral removal steps are critical processing steps for some processes and should be performed within their validated parameters. In other words, regulatory agencies require at least two separate steps such as viral inactivation and viral removal. The intermediate purification and polishing steps are required for separating impurities from the pool of the drug substance. Fig. 1.2 shows the overview of platform downstream process for IgG monoclonal antibody [5]. The Fig. 1.2 explains that polishing steps contain intermediate purification steps.

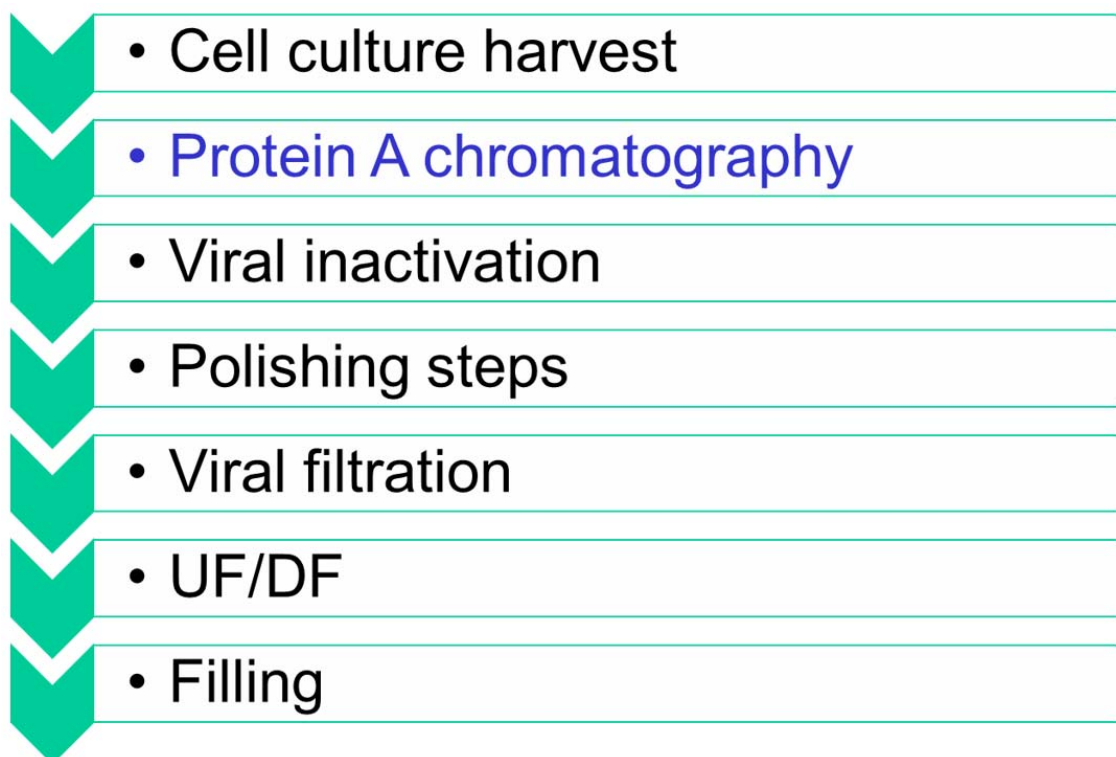


Fig. 1.2. Platform downstream process for IgG monoclonal antibody [5].

1.2 Microporous membranes

Membranes are classified with microfiltration (MF; pore size between 0.05 and 10 μm), ultrafiltration (UF; pore size between 1 and 20 nm) and reverse osmosis (RO; pore size less than 1 nm) according to pore size. In the manufacturing processes such as mAbs and recombinant gene proteins for medical use, MF is almost applied for the prefiltration in order to raise filtration efficiency in UF, and remove bacteria, mycoplasma and cells. UF is often utilized for concentration of the target protein, buffer exchange and virus clearance which is required for biologically derived therapeutics in a process solution. Moreover, a membrane filtration is attractive because it is simple to operate and causes minimal damage, even for products that are highly labile to heat, radiation, or chemical treatment [6]. The greatest interest has been in the application of the pressure-driven processes of MF, UF and virus filtration as shown in Fig. 1.3. Virus filtration, ultrafiltration and nanofiltration shown in Fig. 1.3 put those together as the UF depending on the materials.

	Microfiltration	Virus filtration	Ultrafiltration	Nanofiltration	Reverse Osmosis
Components retained by membrane	Intact cells Cell debris Bacteria	Viruses	Proteins	Divalent ions Amino acids Antibiotics	Amino acids Sugars Salts
Membrane					
Components passed through membrane	Colloids Viruses Proteins Salts	Proteins Buffer components	Amino acids Antifoam Buffer components	Salts Water	Water

Fig. 1.3. Comparison of removal characteristics of different pressure-driven membrane processes [7].

As other characteristics of membranes, there are pore size distribution and membrane types which are important for achieving antifouling properties and dealing with varieties of production scale. High capacity membranes have been developed for the biotechnology industry with varying pore size distribution such as isotropic and anisotropic structures. Isotropic membranes have a uniform structure throughout the depth of the membrane. On the other hand, anisotropic membranes have a graded pore size distribution that varies throughout the depth of the membrane. Thus, anisotropic membranes can retain different particle sizes by different layers within the membrane. As membrane types, there are cartridge type, hollow fiber and flat sheet, and their systems are often introduced in production facilities. In Fig.1.4, the materials of filter are used polypropylene and hydrophilic polyvinylidene fluoride (PVDF). These membranes should be applied repeatedly in accordance with the validated protocol such as the operating conditions of flow velocity, operating pressure, time and cleaning methods.



Fig. 1.4. (A) Microdyn 0.2 µm polypropylene hollow fiber microfiltration system with 174 m² membrane area. (B) Millipore Prostack™ flat sheet membrane system with 186 m² of 0.65 µm pore size hydrophilic PVDF membrane [7].

1.3 Plasma

A plasma is generated by applying energy to an inert gas such as an argon (Ar) in order to reorganize the electronic structure of the species and produce excited species (Ar^*) and ions (Ar^+). The electric field transmits energy to the gas electron, and electronic energy is transmitted to the neutral species by collisions. Most excited species exist in a short time and get to ground state by emitting a photon ($h\nu$). On the other hand, the argon metastable (Ar^m), is the most important active species in the plasma, exist a long time and an approximately energy level of 11.5 eV.

The non-local thermodynamic equilibrium (non-LTE) plasma is often explained with an electron temperature (T_e) and a heavy particle temperature (T_h) [8]. Fig. 1.5 shows the influence of the pressure on the transition from a glow discharge ($T_e = T_h = T_g$) to an arc discharge ($T_e \neq T_h$). T_g means gas temperature. The low pressure plasma (less than 10^{-2} kPa) is non-LTE, because the average kinetic energy of electron is higher than that of heavy particle. Thus, a vacuum pump is often used in order to generate the plasma.

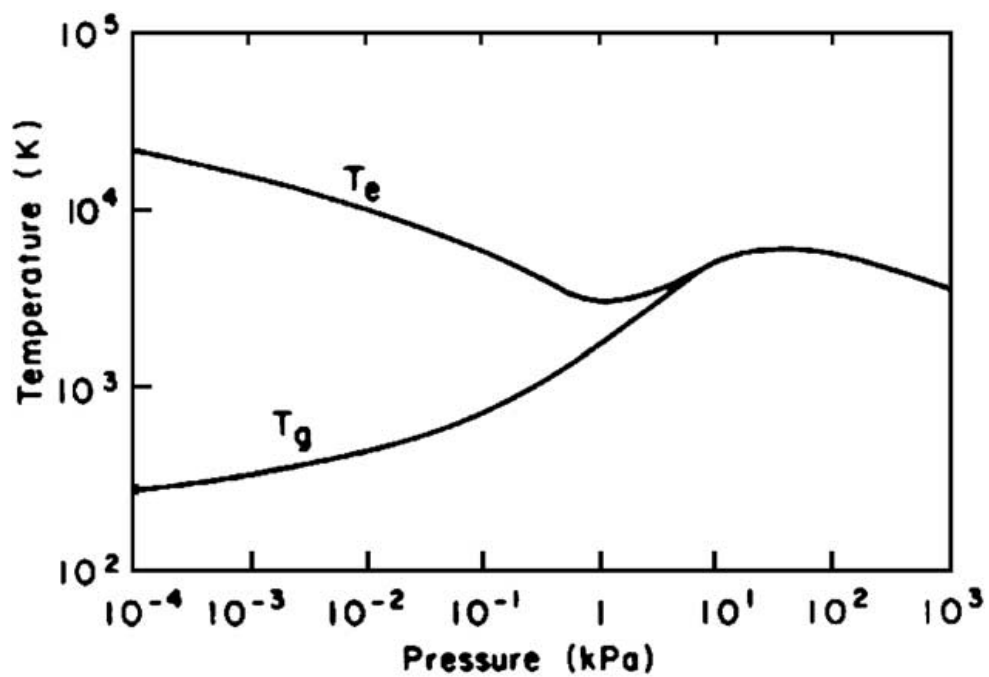


Fig. 1.5. Evolution of the plasma temperature (electrons and heavy particles) with the pressure in a mercury plasma arc [9].

In order to generate the atmospheric pressure low temperature plasma, the excitation frequency plays an important role. Fig. 1.6 shows an example of the variation range for f_{pe} (frequency of the electrons in the plasma) and f_{pi} (ions frequency) in cold plasmas.

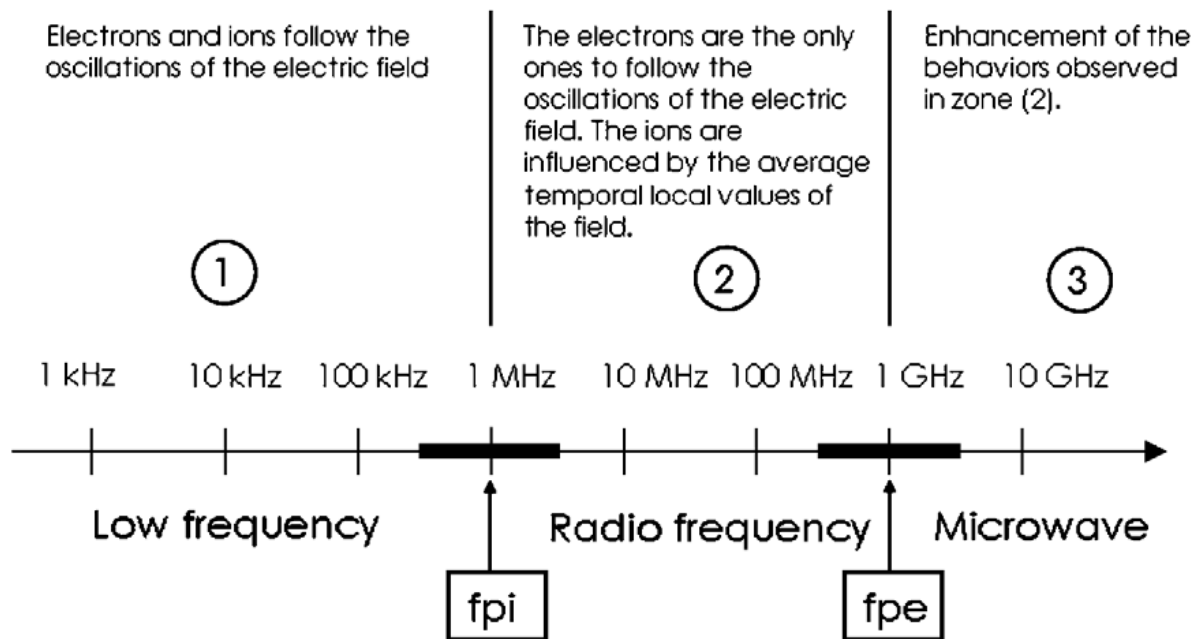


Fig. 1.6. Electrons and ions frequencies in cold plasmas [10].

Moreover, the dielectric barrier discharge (DBD) is the effective application in order to generate the plasma for preventing the heat occurred by the intensive collisions (Fig. 1.7). Although most of the plasma process had been performed in a vacuum container, the application field, such as coatings and sterilizations, has been expanded and opened in laboratories and industries by using the atmospheric pressure low temperature plasma owing to the increase of the treatment speed and area.

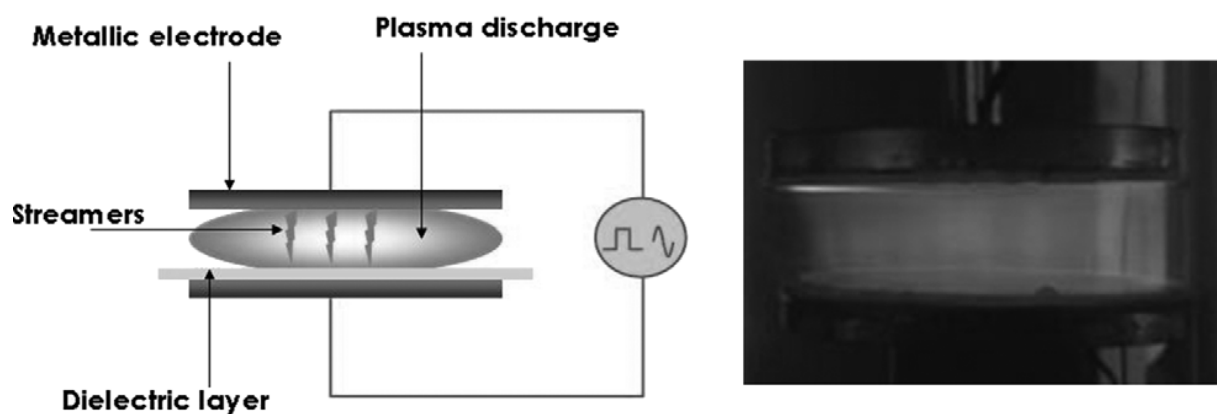


Fig. 1.7. Principle of dielectric barrier discharge (picture: a non-equilibrium diffuse plasma at atmospheric pressure [11]).

The other merit of the plasma at atmospheric pressure is to treat at low temperature. Fig. 1.8 shows the temperature increment profile of the He and Ar plasma jets by the time. Fig. 1.8 was cited from the data measured by the Kuroda Lab. These data indicate that the temperature was 34 °C or less. Therefore, it is preferable to treat the material surface which is vulnerable to heat.

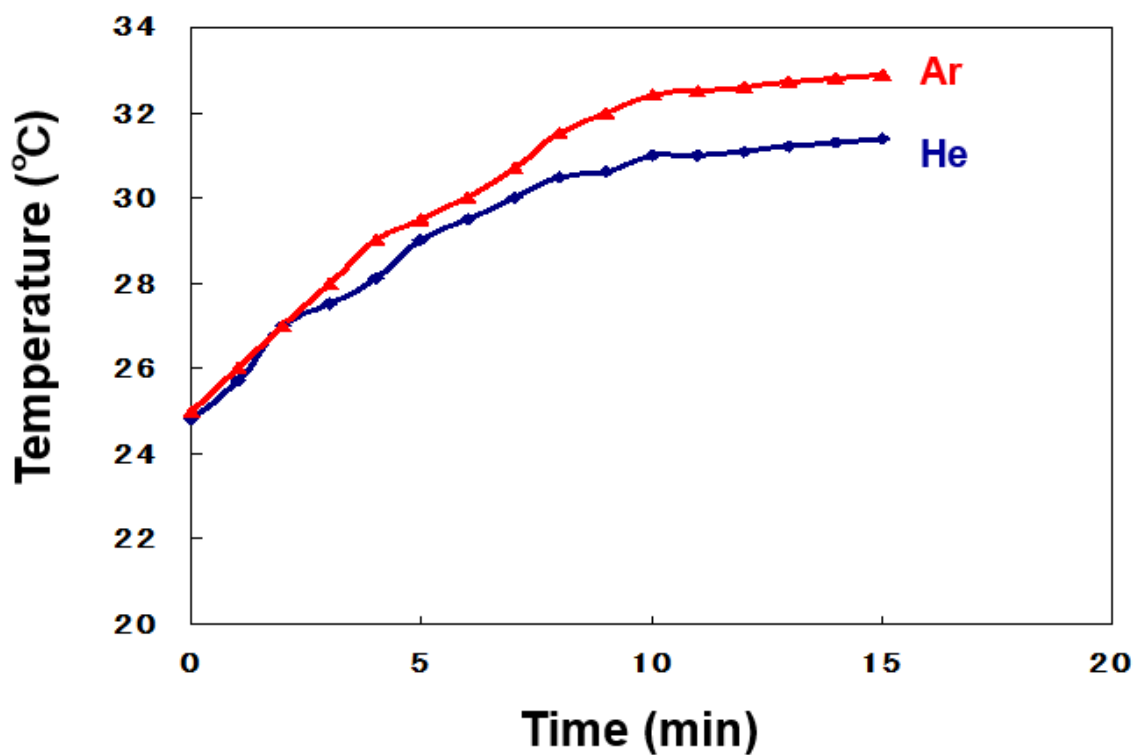


Fig. 1.8. Temperature increment profile of the He and Ar plasma jets by the time.

Plasma treatments have been often used industrially for modifying the surface of materials. Fig. 1.9 shows the concentration of oxygen introduced on the surface of polypropylene (PP) and polystyrene (PS) after the irradiation of the atmospheric pressure low temperature plasma. Fig. 1.9 was also cited from the data measured by the Kuroda Lab. It can be seen that the oxygen was highly detected on the surface of the each material which was treated in jet. Therefore, it is clear that the atmospheric pressure low temperature plasma is effective for proceeding oxidation reactions on the surface of polymer materials in a short time.

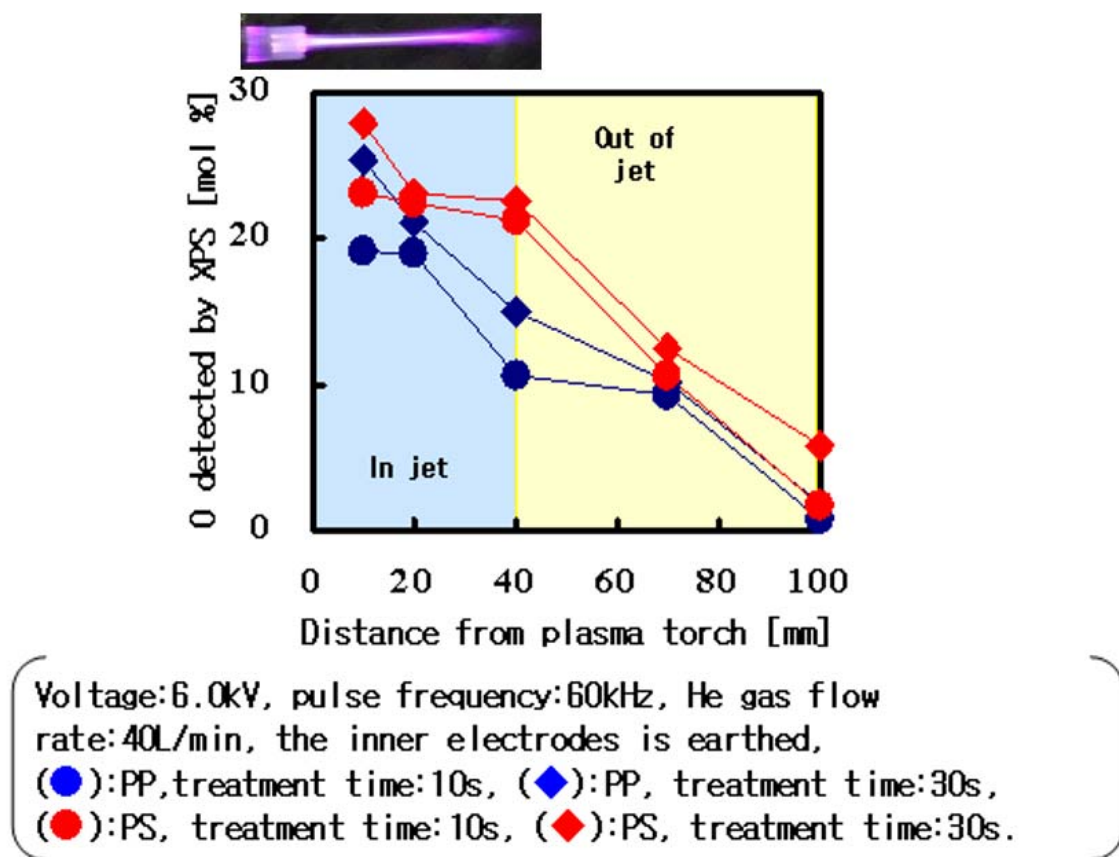


Fig. 1.9. The concentration of oxygen on the surfaces of PP and PS.

1.4 Affinity membranes

In recent years, many functionalized membranes by surface modifications have been reported [12-17]. As reported in the literature [18, 19], there are ion-exchange MF membranes that anion exchange groups are cross-linked with regenerated cellulose membrane, and hydrophobic interaction MF membranes which introduced the phenyl groups, and human γ -globulin adsorption capacity of PVDF hollow fiber affinity membranes containing different amino acid ligands [20]. Therefore, unlike a conventional separation mechanism such as size exclusion, the membrane chromatography is one of the excellent technique of the flow through type that is designed for removing a relatively small amount of impurities such as deoxyribonucleic acid, endotoxin [21], host cell protein, and virus in a production process by peculiar interaction [22, 23]. As different impurities, there are protein aggregates and cleaved products which is a common though undesirable occurrence or post-translational modification. Size exclusion chromatography which is used for preparative separation of mAb aggregates is slow and results in poorly resolved peaks, particularly for higher order aggregates. Lu Wang *et al.* have reported that a hydrophobic interaction membrane chromatography (HIMC) based method was rapidly and efficiently separation and analysis of mAb aggregates [24]. These surface modified membranes are generally offered as a single-use, or disposable in order to reduce cleaning validation requirements in comparison with conventional ion-exchange and hydrophobic interaction chromatography resins. Therefore, the burden of operations would be decreased.

1.5 Objectives and originalities of this study

The final goal of this study was to provide the fundamental technologies for preparation of superior drug products and materials in order to relieve the pains of the patients. As the ways, I have studied to fabricate the model case about alternatives for the operation especially in the core process of the pharmaceutical production by using the latest technologies, or the atmospheric pressure low temperature plasma. In case of production for antibody drugs, Protein A affinity chromatography media are one of the core processes and the media are very expensive materials. Thus, I decided to study for preparing and characterizing Protein A-immobilized membranes. The method for immobilization was adopted the atmospheric pressure low temperature plasma which was considered to modify the surface of membranes mildly. The materials of the membrane were employed PVDF and polyether sulfone (PES) membranes, which are commercially available and often adopted in the pharmaceutical process.

On the other hand, it was thought that the affinity membrane which was directly immobilized with Protein A could be limited to provide the mobility and functionality of Protein A as shown in Fig. 1.10a. The another issue was whether it was capable of fabricating the affinity membranes which was sufficient for adsorbing with more antibodies. Therefore, the graft polymerization was performed on the plasma-treated membranes with reactive monomer which has carboxy group necessary for increasing the ligand density on the affinity membrane, and it was considered to improve the mobility of Protein A due to the flexibility of the polymeric matrix shown in Fig. 1.10b.

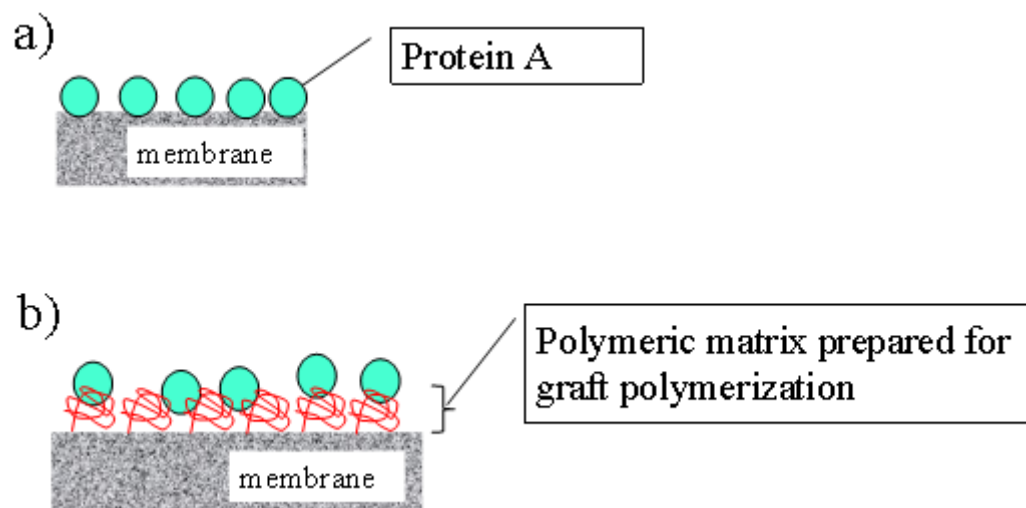


Fig. 1.10. The reason of performing graft polymerization before immobilization of Protein A.

Before performing the tests about the immobilization actually, it was important for understanding the activation mechanism of the surface modified by the plasma chemically to establish the high reproducibility in the preparation. Because plasma treatments are effective to induce functional groups such as oxygen species, but the degradation and unexpected species might generate on the surface at the same time due to the intensity of the plasma deposition and chemical reactions that occurred with the bombardment of the target material, circumambient ingredient and active species of the working gas.

The first goal of this study was to reveal the activation mechanism of the membranes activated by the plasma and immobilize a model protein in order to confirm chemical properties of the membrane surface and the feasibility for preparation. The material of the first study phase was focused on the PVDF membrane. The surface chemical and morphological properties, and activation mechanism of the PVDF membrane were characterized by attenuated total reflection (ATR) Fourier transform infrared (FT-IR) spectroscopic analysis, scanning electron microscopy (SEM) and X-ray photoelectron spectroscopy (XPS), and these findings were described in the chapter 2 [25].

The second goal of this study was to characterize the properties of Protein A-immobilized the membranes. The material of the second study phase was also included the PES membrane. The test samples were used for the hydrophilic PVDF and PES membranes because of considering for applications. The surface chemical and morphological properties and activation mechanism of the PES membrane were

characterized. The adsorption capacities with human immunoglobulin G (IgG) were confirmed according to the monolayer Langmuir model, and the ligand densities on the PVDF and PES membranes were also measured by bicinchoninic acid (BCA) protein assay. These findings were described in the chapter 3 [26].

The most important originalities in this study were to elucidate the activation mechanism on the surfaces of PVDF and PES treated with the atmospheric pressure low temperature plasma chemically. The other originalities were to characterize the functionalities of Protein A-immobilized PVDF and PES membranes and provided the model case for the preparation.

References

- [1] Guide to biological medicines a focus on biosimilar medicines, EuropaBio
- [2] Manufacturing Industries Bureau, Ministry of Economy, Trade and Industry. Report for bio-innovation, June 2010.
- [3] John H. Chon and Gregory Zarbis-Papastoitsis. Advances in the production and downstream processing of antibodies, *New Biotechnology* 2011: Volume 28, Number 5
- [4] John R. Birch, Andrew J. Racher. Antibody production, *Advanced Drug Delivery Reviews* 2006; 58: 671.
- [5] Low D., O'Leary R., Pujar N. S.: Future of antibody purification. *Journal of Chromatography B*, 848, 48-63 (2007).
- [6] Kuriyel Ralf, Zydney Andrew L. Sterile filtration and virus filtration. *Methods Biotechnol* 2000; 9:185.
- [7] Robert van Reis, Andrew Zydney. Bioprocess membrane technology, *Journal of Membrane Science* 2007; 297:16
- [8] Claire Tendero, Christelle Tixier, Pascal Tristant, Jean Desmaison, Philippe Leprince. Atmospheric pressure plasmas: A review, *Spectrochimica Acta Part B* 2006; 61: 2
- [9] M.I. Boulos, P. Fauchais, E. Pfender, *Thermal Plasmas: Fundamental And Applications*. Volume I, Plenum Press, New York, ISBN: 0-306-44607-3, 1994, 452 pp.
- [10] F. Arefi-Khonsari, De'po^ t et traitement des polyme`res par proce`de`s plasma, *Formation Continue INPG– 17e`me session –Traitements de Surface par Plasmas*, 24–28 Mars 2003, Grenoble, France, 2003

- [11] Applied Plasma Technology Laboratory: Old Dominion Center for Bioelectronics [on line]. Available on: <http://www.ece.odu.edu/~mlarouss/> (consulted on 06.05.04).
- [12] Ritchie Stephen MC, Kissick Kyle E, Bachas Leonidas G, Sikdar Subhas K, Parikh Chetan, Bhattacharyya Dibakar. Polycysteine and other polyamino acid functionalized microfiltration membranes for heavy metal capture. *Environ Sci Technol* 2001; 35:3252.
- [13] Ritchie SMC, Bachas LG, Olin T, Sikdar SK, Bhattacharyya D. Surface modification of silica- and cellulose-based microfiltration membranes with functional polyamino acids for heavy metal sorption. *Langmuir* 1999; 15:6346.
- [14] Singh Nripen, Husson Scott M, Zdyrko Bogdan, Luzinov Igor. Surface modification of microporous PVDF membranes by ATRP. *J Membr Sci* 2005; 262:81.
- [15] Nasef Mohamed Mahmoud, Güven Olgun. Radiation-grafted copolymers for separation and purification purposes: status, challenges and future directions. *Prog Polym Sci* 2012; 37:1597.
- [16] Ulbricht Mathias. Advanced functional polymer membranes. *Polymer* 2006; 47:22.
- [17] Han Man Jae, Baroña Garry Nathaniel B, Jung Bumsuk. Effect of surface charge on hydrophilically modified poly (vinylidene fluoride) membrane for microfiltration. *Desalination* 2011; 270:76.
- [18] Kalbfuss Bernd, Wolff Michael, Geisler Liane, Tappe Alexander, Wickramasinghe Ranil, Thom Volkmar, *et al.* Direct capture of influenza A virus from cell culture supernatant with sartobind anion-exchange membrane adsorbers. *J Membr Sci* 2007; 299:251.
- [19] Kosior Anna, Antošová Monika, Faber Rene, Villain Louis, Polakovič Milan. Single-component adsorption of proteins on a cellulose membrane with the phenyl ligand for hydrophobic interaction chromatography. *J Membr Sci* 2013; 442:216.

- [20] Sun Haixiang, Zhang Lin, Chai Hong, Yu Ji, Qian Hua, Chen Huanlin. A study of human γ -globulin adsorption capacity of PVDF hollow fiber affinity membranes containing different amino acid ligands. *Sep Purif Technol* 2006; 48:215.
- [21] Zhang Mo, Zhang Lin, Cheng Li-Hua, Xu Kun, Xu Qiu-Ping, Chen Huan-Lin, *et al.* Extracorporeal endotoxin removal by novel l-serine grafted PVDF membrane modules. *J Membr Sci* 2012; 405e406:104.
- [22] Teeters MA, Conrardy SE, Thomas BL, Root TW, Lightfoot EN. Adsorptive membrane chromatography for purification of plasmid DNA. *J Chromatogr* 2003; 989:165.
- [23] Woo Maybelle, Khan Navid Z, Royce Jonathan, Mehta Ushma, Gagnon Brian, Ramaswamy Senthil, *et al.* A novel primary amine-based anion exchange membrane adsorber. *J Chromatogr* 2011; 1218:5386.
- [24] Wang Lu, Ghosh Raja. Fractionation of monoclonal antibody aggregates using membrane chromatography. *J Membr Sci* 2008; 318:311.
- [25] Naohisa Akashi and Shin-ichi Kuroda.: Protein immobilization onto poly (vinylidene fluoride) microporous membranes activated by the atmospheric pressure low temperature plasma, *Polymer*, 55, 2780-2791 (2014).
- [26] Naohisa Akashi and Shin-ichi Kuroda.: Preparation and characterization of Protein A-immobilized PVDF and PES membranes, *eXPRESS Polymer Letters*, in press.

Chapter 2 Protein immobilization onto polyvinylidene fluoride microporous membranes activated by the atmospheric pressure low temperature plasma

2.1 Introduction

PVDF is one of the fluorocarbon polymers which can be used widely as a membrane material [1]. Hydrophobic PVDF membranes have a characteristic property which substantially interacts with proteins by hydrophobic interaction, so it is suitable for analysis applications which is identified or detected the small amount of target protein. On the other hand, hydrophilized PVDF membranes have been mainly adopting in the manufacturing processes for obtaining pharmaceutical drug substances or products for biologics.

On the other hand, as a method of surface modifications, there is the dry process that is clean and energy saving, and plasma processing [2-7], gamma irradiation [8, 9], ultraviolet irradiation [10-14], photo-irradiation [15, 16] are reported. In case of plasma processing with vacuum, there are some problems, for example, it is necessary to use a powerful pump and robust chamber in order to generate a vacuum condition, and it takes time before reaching a vacuum. On the contrary, in the atmospheric pressure low temperature plasma [17-21], it does not need equipment for vacuum processing, and partial surface treatment is possible. It is also applicable for the surface treatment of

materials of low thermal stability because of low temperature processing.

The first goal of this study was to reveal the activation mechanism on the PVDF membrane activated by the plasma and immobilize a model protein on membranes in order to confirm chemical properties of the membrane surface and the feasibility for preparation. The surface chemical and morphological properties of the membrane were characterized by ATR FT-IR spectroscopic analysis, SEM and XPS, and findings were described in this chapter.

2.2 Experimental

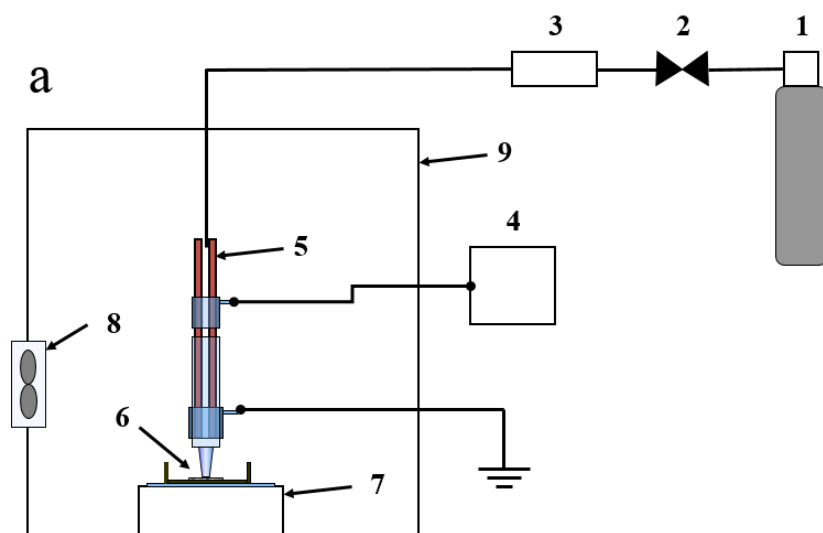
2.2.1 Materials

Hydrophobic membrane PVDF (Durapore[®], 0.45 μm pore size) was purchased from Merck Millipore Corp. (Darmstadt, Germany) which was commercially named HVHP01300. *N*-Hydroxysulfosuccinimide (Sulfo-NHS), 1-(3-(dimethylaminopropyl)-3-ethylcarbodiimide HCl (EDC) and 2-(*N*-morpholino)ethanesulfonic acid (MES) were purchased from ProteoChem, Inc. Acrylic acid (AA) monomer and bovine serum albumin (BSA) were purchased from Sigma-Aldrich, Inc. (MO, United States). AA was distilled in nitrogen atmosphere prior to use. PBS (-) was purchased from Nissui Pharmaceutical Co., Ltd (Tokyo, Japan). The purity of the argon gas used was in excess of 99.99%. Distilled water was used in all experiments.

2.2.2 Plasma reactor and plasma treatments

Fig. 2.1 shows the equipment used in this study. It consists of a high frequency pulse power supply, a gas supply unit and the cold atmospheric pressure plasma torch (CAPPLAT) (Fig. 2.1a) [22, 23]. The CAPPLAT has a cylindrical structure in which the plasma is generated. The plasma is blown out through the end of the CAPPLAT which consists of two co-axial cylindrical electrodes (Fig. 2.1b). The inner electrode, a copper tube (OD: 8 mm, ID: 7 mm), is connected to the power supply. The outer electrode (thickness: 1 mm, length: 20 mm) is made of aluminum and grounded. As a dielectric barrier, a silicone tube (thickness: 2.5 mm) is placed between the two

electrode. The outlet of the CAPPLAT is embedded in the edge of a perforated silicone tube.



(1) argon gas cylinder; (2) valve; (3) mass flow meter; (4) power supply; (5) torch; (6) substrate; (7) stage; (8) exhaust fan; (9) reaction chamber

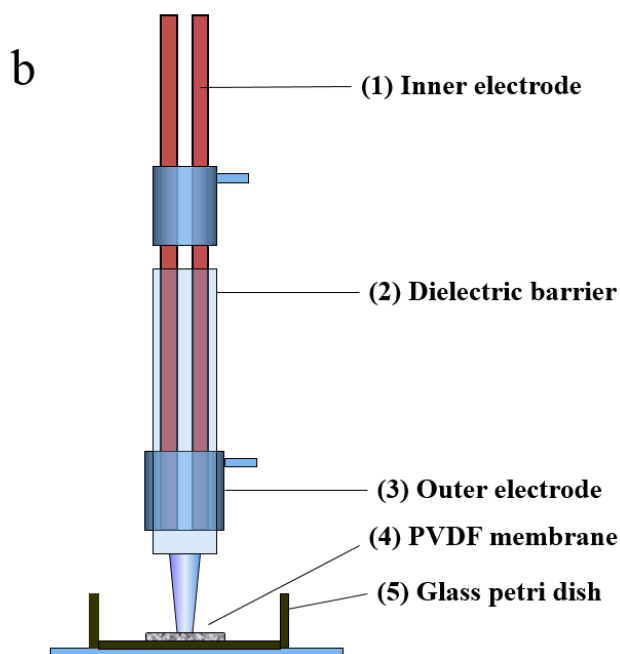


Fig. 2.1. Schematic structure of (a) plasma reactor and (b) CAPPLAT

2.2.3 Immobilization procedure

Prior to the surface modification experiment, the PVDF membrane was rinsed with ethanol in an ultrasonic washer and dried at room temperature for 12 h. For plasma treatment of the PVDF membrane, argon gas was fed into the CAPPLAT at a flow rate of 5 L min⁻¹ and the plasma was generated under the following conditions; applied voltage of ± 4 kVp-p, frequency of 20 kHz, treatment time of 180 s and duty cycle of 50%. The PVDF membrane was treated with plasma at the position of 20 mm away from the torch end. Subsequently, the PVDF membrane was exposed to air for 20 min. The air-exposed membrane was immersed in an aqueous solution containing 20% (v/v) of AA monomer. After bubbling with nitrogen for 20 min to remove dissolved oxygen, the ampoule was sealed and heated at 70°C to initiate graft polymerization. The PVDF membrane grafted with polyacrylic acid (hereafter called PVDF-g-PAA) was rinsed with distilled water several times to remove nongrafted monomers for 12 h. Graft yield was determined from initial and final weight after drying obtained using a balance measuring to an accuracy of 0.05 mg.

The degree of grafting was calculated as the weight increase of the membrane according to the following equation [24, 25]:

$$\text{Degree of Grafting (G\%)} = \frac{W_g - W_o}{W_o} \times 100$$

where W_g is the weight of the grafted membrane and W_o is the weight of the membrane.

BSA was grafted on PVDF-g-PAA membrane surface using the EDC/NHS method. The

PVDF-g-PAA membrane was activated with 4 mmol L⁻¹ EDC, 10 mmol L⁻¹ Sulfo-NHS in 100 mmol L⁻¹ MES, 500 mmol L⁻¹ NaCl pH 6.0 buffer for 15 min at room temperature. The conjugation of BSA was carried out in a solution of 1 mg mL⁻¹ BSA in 100 mmol L⁻¹ MES, 500 mmol L⁻¹ NaCl pH 6.0 buffer under mild agitation for 3 h at room temperature. The membrane (hereafter called PVDF-g-PAA-BSA) was rinsed with a solution of PBS (-) to remove loosely absorbed BSA and MES buffer for 12 h.

2.2.4 Physical and chemical surface characterization

KYOWA KAIMEN KAGAKU CA-D (Saitama, Japan) was used to measure static contact angle of water of the membranes using a sessile drop method. The angles reported were reliable to $\pm 1^\circ$. For each angle reported, at least five sample readings from different surface locations were averaged.

To study the surface chemical composition changes of the membranes, ATR FT-IR spectroscopic investigations were carried out with a Nicolet MAGNA IR560 spectrometer using a Ge crystal (Thermo Fisher Scientific Inc., MA, United States). The spectra were measured in the wave number range of 1000 - 4000 cm⁻¹. The spectra were collected by cumulating 64 scans at a resolution of 4 cm⁻¹. All ATR-FTIR spectra were recorded at ambient temperature.

XPS was used to analyze the chemical composition of the untreated and functionalized PVDF membranes and was performed on a Kratos AXIS Nova spectrometer (Manchester, United Kingdom) using a monochromatized Al K α X-ray source (1486.6 eV photons). The base pressure in the analytical chamber was maintained at 10⁻⁸ Torr or

lower during each measurement. All measurements were made at a photoelectron takeoff angle of 45°. The Kratos charge neutralizer system was used on all specimens. The X-ray source was run at a reduced power of 150 W (15 kV and 10 mA). The samples were mounted on the standard sample plate by means of adhesive tapes. Survey scan analyses were carried out at a constant dwell time of 100 ms, pass energy of 160 eV and energy resolution of 1 eV. High resolution analyses were carried out at a constant dwell time of 200 ms, pass energy of 20 eV and energy resolution of 0.1 eV. All binding energies (BEs) were referenced to the C1s hydrocarbon peak at 286.4 eV. Spectra were analyzed using XPSPEAK software (version 4.1). Curve fitting of the high resolution spectra used 30% Gaussian/70% Lorentzian mixed line shapes for each component.

2.2.5 Membrane morphology

The surface and cross-section morphologies of the membranes were examined by SEM, using a Hitachi S-3000N electron microscope. The samples were mounted on the standard sample plate by means of adhesive tapes. A thin layer of Pt was sputtered on the sample surface prior to the SEM measurement. For cross-sectional view studies, the membrane was fractured under liquid nitrogen. A thin layer of platinum was sputtered onto the cross-sectional surface prior to the SEM measurement. The SEM measurements were performed at an accelerating voltage of 15.0 kV.

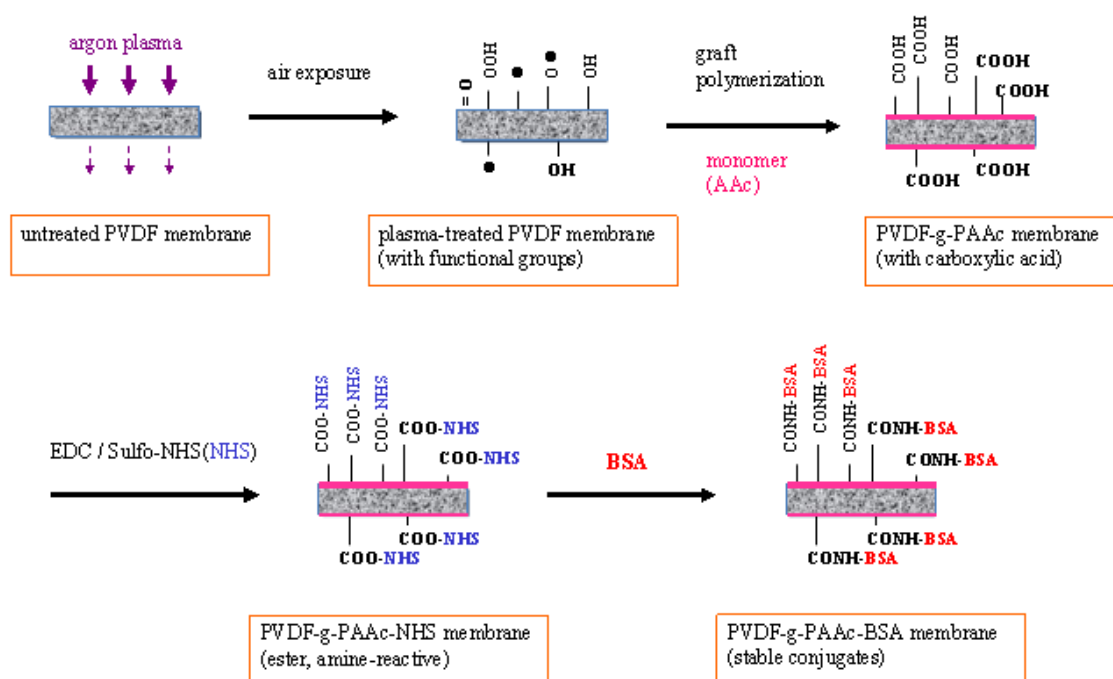
The cross-sectional view of the PVDF-g-PAA membrane was also measured by energy dispersive X-ray spectroscopy (EDX) using a Horiba EX-200K to estimate the distribution profile of the grafted AA. The sample was immersed in an aqueous solution of 1.0 wt % potassium hydroxide at 25°C for 24 h and then washed with water. The membrane was fractured prior to the measurement.

An atomic force microscopy (AFM, Seiko Instruments SPA-400) was also used to further study the surface topography change of the membrane. AFM images were acquired in the dynamic force mode with a cantilever (SI-DF20, Seiko Instruments). To investigate surface roughness of each sample, it was calculated average roughness (R_a).

$$R_a \text{ [nm]} = \frac{1}{L} \int_0^L |F(x)| dx$$

2.3 Results and discussion

Scheme 2.1 shows a schematic diagram illustrating the process of surface modifications. As a first step, the surface of PVDF membrane was treated with argon plasma. The plasma-treated samples are generally exposed to air in order to generate peroxide and hydroperoxide initiator species. AA was graft polymerized in the solution by thermal initiation. After EDC/Sulfo-NHS reaction step, BSA was conjugated on the carboxy groups of the PVDF-g-PAA membrane surface. Subsequently, PVDF-g-PAA-BSA membrane was fabricated for immobilizing onto the aminated surface of the PVDF-g-PAA-NHS membrane.



Scheme 2.1. Schematic illustration of the surface modifications by graft polymerization of AA.

2.3.1 Hydrophilicity characterization

Plasma contains activated species which are able to initiate chemical and physical reactions on the solid surfaces of polymers. When polymers are exposed to plasma, essentially degradation reactions such as polymer chain scission and cross-linking initiate. On the other hand, functional groups for example hydroperoxide and carboxy will be formed on the polymer surface. Fig. 2.2 shows the results of contact angle of water on the PVDF membrane surface, treated by argon plasma, as a function of plasma exposure time from 30 to 300 s and a voltage of $\pm 2.8 - 5.0$ kVp-p.

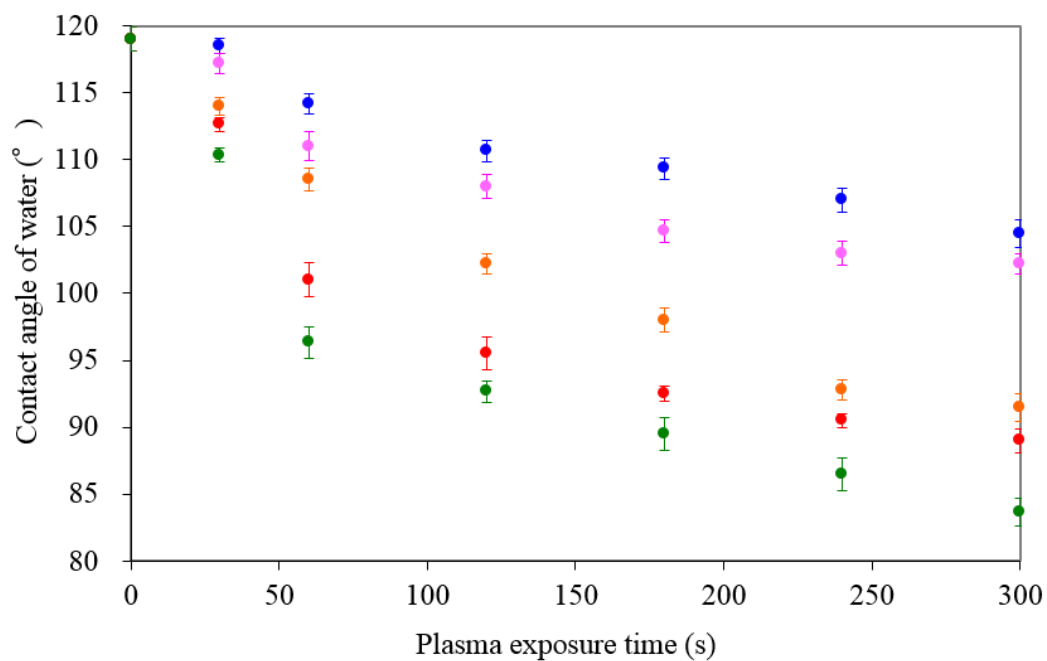


Fig. 2.2. Contact angle of water on PVDF membrane surface treated with argon plasma as a function of plasma exposure time and voltage: (blue) ± 2.8 kVp-p, (pink) ± 3.5 kVp-p, (orange) ± 4.0 kVp-p, (red) ± 4.5 kVp-p, (green) ± 5.0 kVp-p. Data are presented as means \pm SD.

Beforehand, I confirmed that the contact angle on plasma-treated PVDF membrane before and after ethanol rinsing had less difference. The contact angle of the non-treated PVDF membrane was about value 119°. The contact angle on the exposed samples was reduced with increasing voltage. It was indicated that the plasma treatment could modify the PVDF membrane surface from hydrophobic to hydrophilic.

The contact angle of PVDF membrane treated with less than ± 3.5 kVp-p for the same exposure time, decreased slowly reaching a similar value, and the appearance did not change from untreated samples. On the other hand, the contact angle of samples treated with ± 4.0 kVp-p decreased almost linearly in the course of processing time, and the surface of the sample treated directly for more than 240 s exhibited a slightly burnt area, which means it contained a little amount of degradation products. In case of samples modified with more than ± 4.5 kVp-p, the contact angle decreased rapidly up to 60 s. Beyond 60 s the contact angle decreased gradually. However, the appearance of the samples was intensively burnt after 60 s. From these results, I realized that plasma treatment of more than ± 4.5 kVp-p led heavy etching reaction, and plasma treatment during 30 - 180 s and $\pm 2.8 - 4.0$ kVp-p could prevent the etching reaction. Hence, I recognized that the treatment time of 180 s and the voltage of ± 4.0 kVp-p were the most effective condition for mild surface modification.

2.3.2 Dependence of the degree of grafting on reaction conditions

PAA was grafted onto the plasma-treated PVDF membrane surface by thermal polymerization method. The grafting yield for a typical plasma-induced free radical polymerization depends on some factors, such as plasma treatment time, plasma power, monomer concentration, reaction temperature, reaction time. In this work, the attention has been focused on the following factors: monomer concentration, reaction temperature, and reaction time.

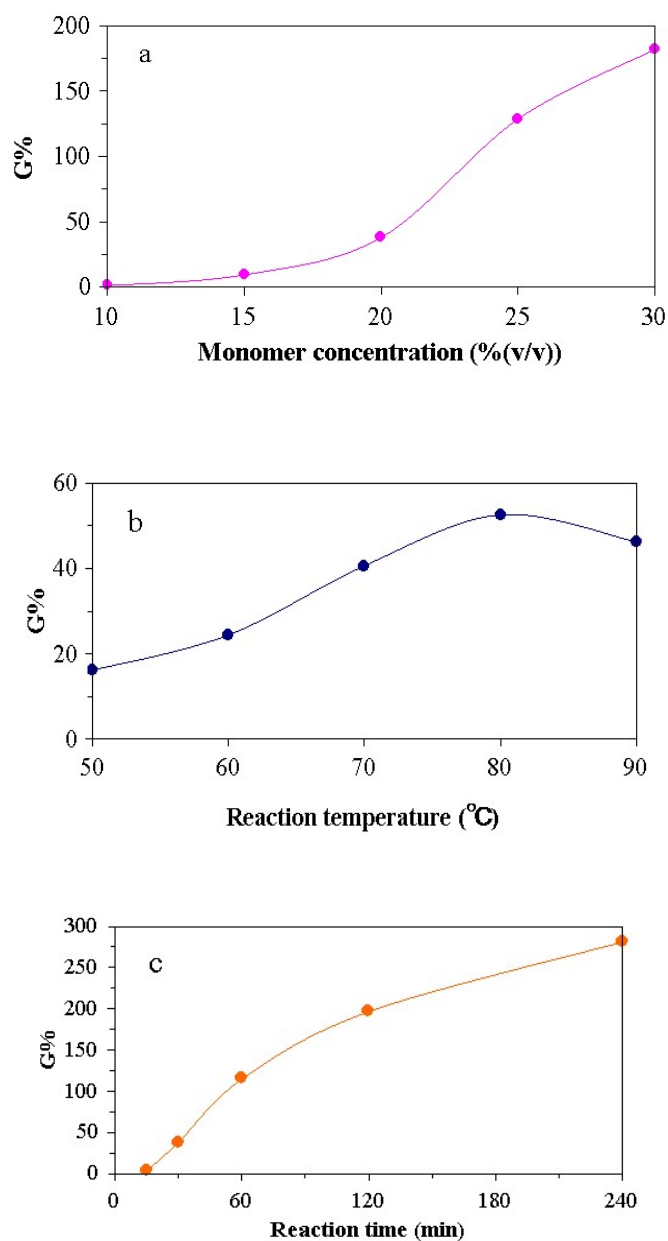


Fig. 2.3. The effect of (a) monomer concentration (treatment: 30 min, 70°C), (b) reaction temperature (treatment: 20% (v/v) AA, 30 min) and (c) reaction time (treatment: 20% (v/v) AA, 70°C) on the grafting yield of PAA. Data are presented as means from 3 independent substrates.

First of all, Fig.2.3a shows the effect of monomer concentration from 10 - 30% (v/v) on the grafting yield of PAA. The grafting yield increased with increasing the monomer concentration, especially more than 20% (v/v). Secondly, Fig. 2.3b indicates the effect of polymerization reaction temperature from 50 - 90°C. The grafting yields increased gradually depending on increasing the reaction temperature up to 80°C, and then decreased after passing through a maximum. Thirdly, Fig. 2.3c represents the effect of polymerization reaction time. The grafting yield increased with increasing the reaction time. It was found that the graft yield of sample treated with monomer 20% (v/v) for 60 min (Fig. 2.3c) was approximately the same value as that of the treated with 25% (v/v) for 30 min (Fig. 2.3a). Furthermore, I realized that monomer concentration and treatment time should be controlled especially as graft conditions.

If the amount of PAA chains on the membrane surface, including the pore surface is larger, the yield of protein immobilization will decrease because of the limited surface area. Considering the scale-up of this polymerization process, it was thought that lower monomer concentration, treatment time and temperature would be preferable in terms of cost effectiveness. Therefore, I decided that the monomer concentration of 20% (v/v), reaction time of 30 min and temperature of 70°C were the optimum conditions for the graft polymerization.

2.3.3 Structure characterization of the membranes by ATR-FTIR analysis

Fig. 2.4 shows the respective ATR-FTIR spectra of (a) untreated PVDF membrane, (b) PVDF membrane treated with argon plasma, PVDF-g-PAA membranes grafted with AA for (c) 15 min, (d) 30 min, and PVDF-g-PAA-BSA membranes covalently immobilized with the BSA concentration of (e) 0.04 mg mL^{-1} , (f) 1.00 mg mL^{-1} .

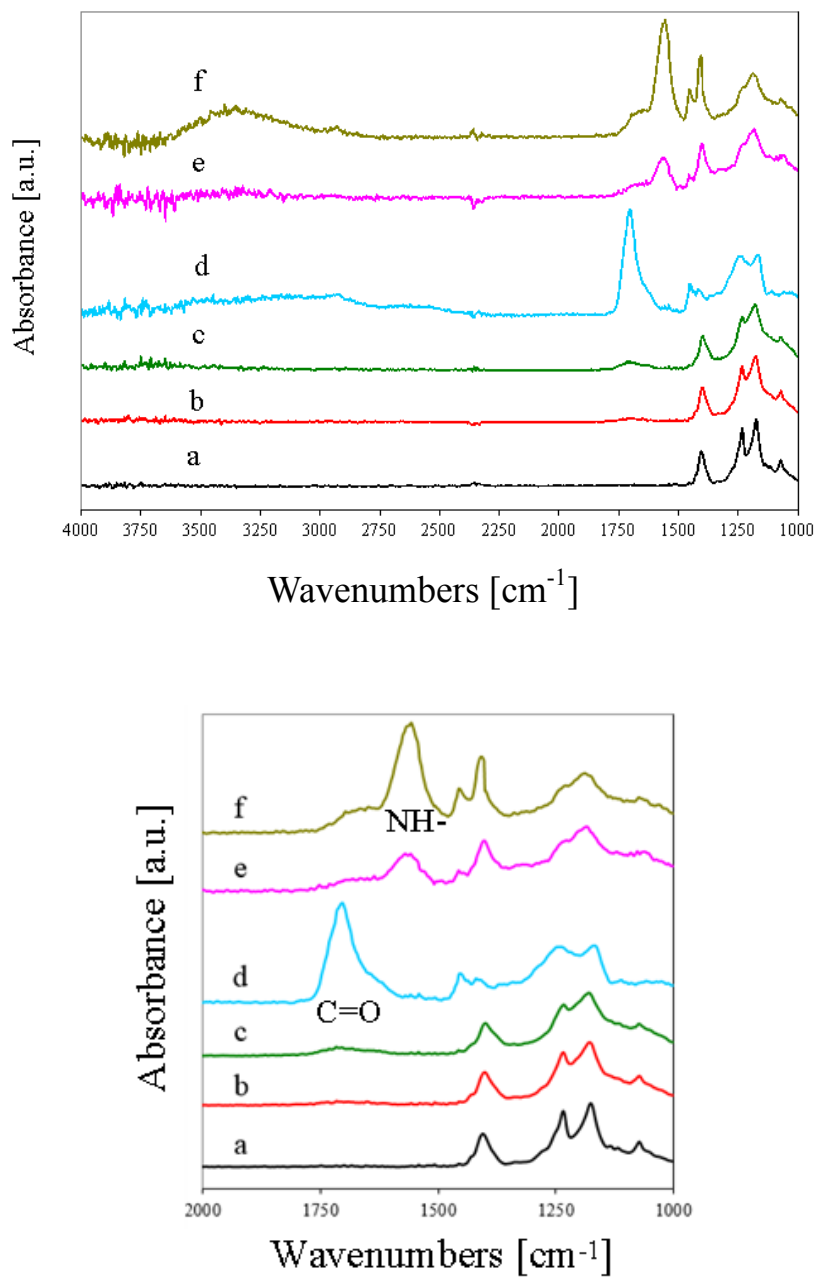


Fig. 2.4. ATR-FTIR spectra of (a) untreated PVDF membrane, (b) PVDF membrane treated with argon plasma (treatment: ± 4.0 kVp-p, 180 s), PVDF-g-PAA membranes grafted with AA for (c) 15 min, (d) 30 min (treatment: 20% (v/v) AA, 70°C), and PVDF-g-PAA-BSA membranes covalently immobilized with the BSA concentration of (e) 0.04 mg mL^{-1} , (f) 1.00 mg mL^{-1} (treatment: 3.0 h).

For comparison purpose, the ATR-FTIR spectrum of the untreated PVDF membrane is shown in Fig. 2.4. The absorption bands at 1070 - 1236 cm^{-1} are characteristic bands of CF_2 functional group of PVDF (Fig. 2.4a). The ATR-FTIR spectrum of the PVDF membrane treated with argon plasma contained a weak absorption band at 1707 cm^{-1} which was associated with C=O stretching of the carbonyl group (Fig. 2.4b).

The ATR-FTIR spectrum of the PVDF-g-PAA membrane grafted with AA for 30 min (Fig. 2.4d) appeared with stronger, C=O absorption stretching band that compared with the sample grafted for 15 min (Fig. 2.4c). It was proved that the grafting yield increased depending on the reaction time. The ATR-FTIR spectrum of the PVDF-g-PAA membrane grafted with AA for 30 min was also exhibited a broad OH stretching absorption band between 3300 and 2500 cm^{-1} . It was suggested that polyacrylic acid chains were successfully grafted onto the surface of the PVDF membrane qualitatively. The acid function of the PVDF-g-PAA membrane must be activated by EDC to react with the BSA amino group.

The ATR-FTIR spectra of the PVDF-g-PAA-BSA membrane shows a characteristic -NH stretching absorption band. Especially, the ATR-FTIR spectrum of the PVDF-g-PAA-BSA membrane covalently functionalized with the BSA concentration of 1.00 mg mL^{-1} (Fig. 2.4f) was found having a stronger NH-deformation vibration at 1554 cm^{-1} that compared with the sample immobilized with the BSA concentration of 0.04 mg mL^{-1} (Fig. 2.4e). It was suggested that the immobilizing yield increased with the BSA concentration and BSA were suitably conjugated onto the surface of the PVDF-g-PAA membrane largely. Furthermore, broad absorption bands attributed to primary amino groups with maximum at 3400 cm^{-1} were observed (Fig. 2.4f). On the

other hand, the bands corresponding to the carboxylic acids and CF_2 functional group indicated a weak absorption.

2.3.4 Structure characterization of the membranes by XPS analysis

The XPS survey spectra of (a) untreated PVDF membrane, (b) PVDF membrane treated with argon plasma and (c) PVDF-g-PAA membranes are shown in Fig. 2.5.

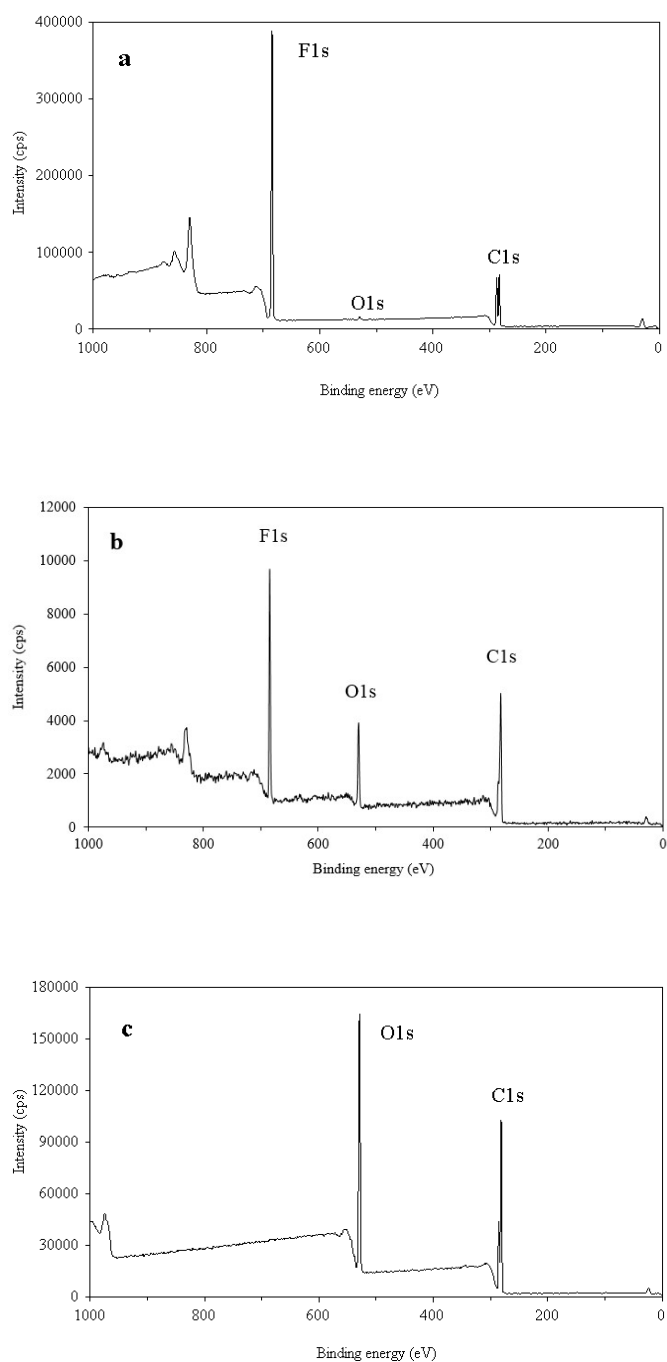


Fig. 2.5. XPS survey scan of (a) untreated PVDF membrane, (b) PVDF membrane treated with argon plasma (treatment: ± 4.0 kVp-p, 180 s) and (c) PVDF-g-PAA membranes (treatment: 20% (v/v) AA, 70°C, 30 min).

Two peaks at BEs of 286 and 291 eV attributable to C1s and a strong peak at BE of 688 eV attributable to F1s were observed in the XPS survey scan spectrum of the non-treated hydrophobic PVDF membrane (Fig. 2.5a). The XPS survey scan spectrum of the PVDF membrane treated with argon plasma consisted of peaks at BEs of 286, 291, 534, and 688 eV, attributable to C1s, C1s, O1s, and F1s, respectively (Fig. 2.5b). On the other hand, the result of the XPS measurement onto PVDF-g-PAA membrane consisted of peaks at BEs of 285, 289, and 533 eV, attributable to C1s, C1s, and O1s, respectively (Fig. 2.5c). It shows that successful grafting of PAA on the plasma-treated membrane was performed since the fluorine content on the surface decreased substantially after grafting.

Atomic composition for the PVDF membrane surfaces modified by argon plasma was estimated from relative intensities of C1s, F1s, and O1s high resolution spectra. Results of XPS analysis for the F/C and O/C atom ratios of the PVDF membrane surface treated with argon plasma are summarized in Table 2.1.

Table 2.1

Atomic ratios of PVDF membrane surface exposed to argon plasma.

Plasma treatment			Atomic ratio		Defluorination
Voltage	Flow rate	Exposure	F/C	O/C	
[\pm kVp-p]	[L min ⁻¹]	time [s]			[%]
-	-	-	1.01	0.01	0
4.0	5	60	0.50	0.16	50
4.0	5	180	0.38	0.20	62
4.0	5	300	0.31	0.20	69
2.8	5	180	0.58	0.14	43
4.0	5	180	0.38	0.20	62
5.0	5	180	0.32	0.21	68
4.0	4	180	0.42	0.19	58
4.0	5	180	0.38	0.20	62
4.0	6	180	0.43	0.18	57

The weak peak at BEs of 533 eV on the survey spectrum of untreated PVDF, attributable to O1s signal, confirmed that the PVDF surface was partially oxidized. However, the O/C atom ratio for the untreated PVDF was 0.01, so it was considered to be low level. All plasma-treated PVDF membrane surfaces showed lower F/C atom ratio than the untreated PVDF surface, and higher O/C atom ratio. In other words, a reduction in fluorine intensity occurred together with an increase in oxygen intensity and relative increase in the carbon. These changes indicate that the plasma exposure led to defluorination including dehydrofluorination and oxidation reactions on the PVDF membrane surfaces.

In this work, I investigated the influence of defluorination and oxidation on the plasma treatment time, applied voltage and flow rate of argon gas. Firstly, defluorination estimated from the F/C atom ratio increased by 50% in 60 s, 62% in 180 s, and 69% in 300 s at ± 4.0 kVp-p compared to untreated PVDF. Secondly, defluorination resulted in 43% at ± 2.8 kVp-p, 62% at ± 4.0 kVp-p, and 68% at ± 5.0 kVp-p in 180 s compared to untreated PVDF. Therefore, with increasing the treatment time and voltage, defluorination was gradually in progress. It was also confirmed that defluorination was occurred even at the minimum voltage of ± 2.8 kVp-p when plasma could be formed. Likewise, oxidation reaction estimated from the O/C atom ratio was also progressed by increasing the rate of the plasma treatment time and applied voltage, however oxidation was approximately the same beyond 180 s or ± 4.0 kVp-p. Finally, as a consequent of evaluating the effect of flow rate of argon gas on defluorination and oxidation, defluorination was 58% at 4 L min^{-1} , 62% at 5 L min^{-1} , and 57% at 6 L min^{-1} for 180 s compared to untreated PVDF. Similarly, oxidation was the most progressed in 20% at 5

L min^{-1} , whereas it was almost at the same level between 4 L min^{-1} and 6 L min^{-1} . Collectively, it was concluded that the most effective flow rate of argon gas was 5 L min^{-1} to abstract fluorine atoms from untreated PVDF and produce reactive sites on the membrane surface for further modification.

To discuss defluorination, dehydrofluorination and oxidation reactions in detail, I investigated the data of narrow scanning C1s and O1s core level spectra. Fig. 2.6 shows C1s and O1s spectra for untreated PVDF membrane, PVDF membrane treated with argon plasma and PVDF-g-PAA membrane. The decomposed peaks were illustrated in dotted lines.

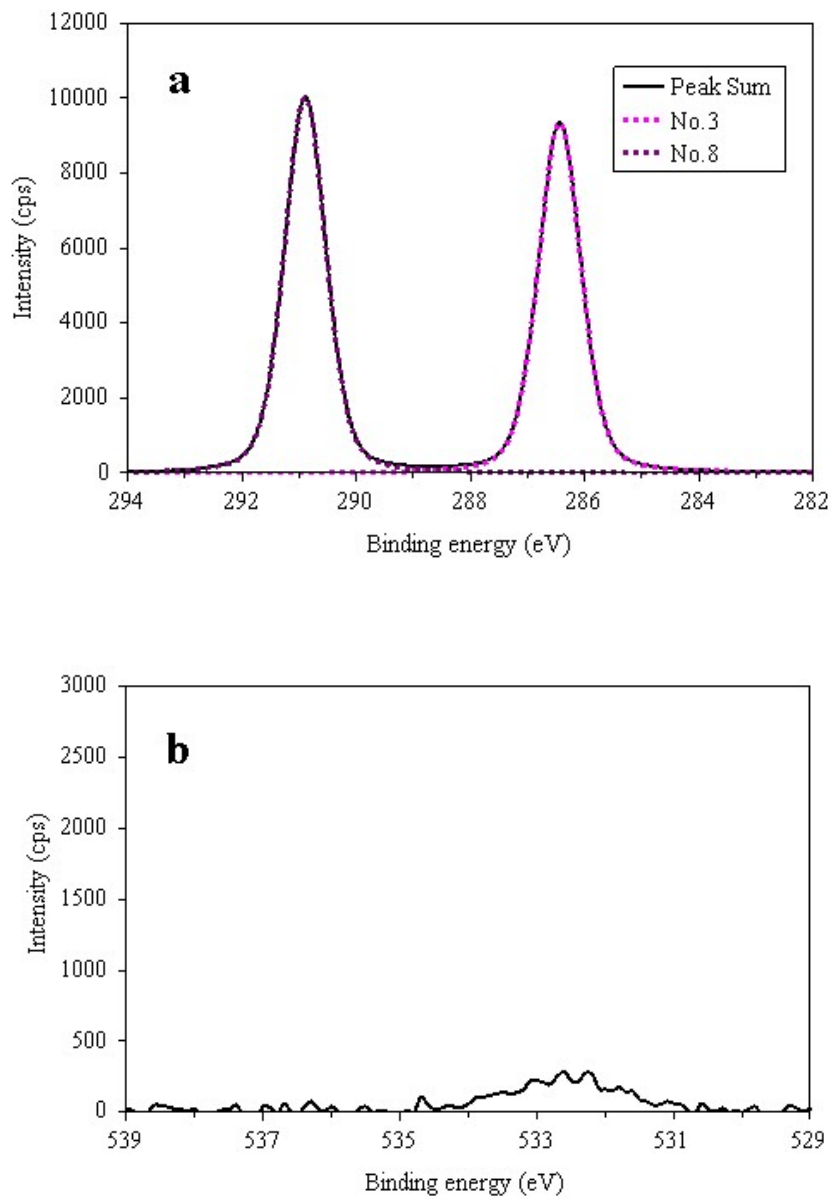


Fig. 2.6. High resolution XPS spectra of C1s (a) and O1s (b) of untreated PVDF membrane. The peak numbers in these figures corresponds to the Peak No. of Table 2.2.

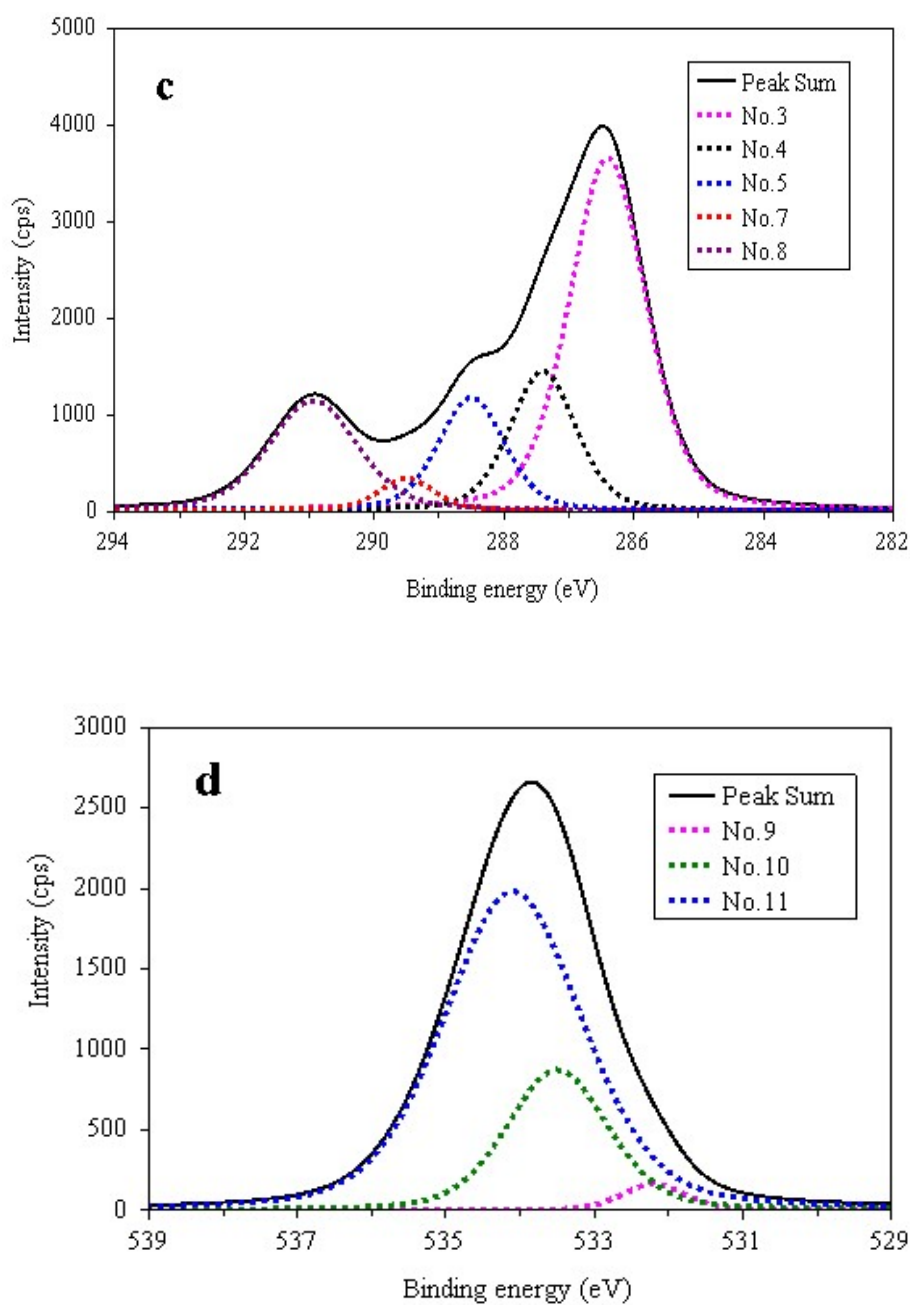


Fig. 2.6. High resolution XPS spectra of C1s (c) and O1s (d) of PVDF membrane treated with argon plasma (treatment: ± 4.0 kVp-p, 180 s). The peak numbers in these figures corresponds to the Peak No. of Table 2.2.

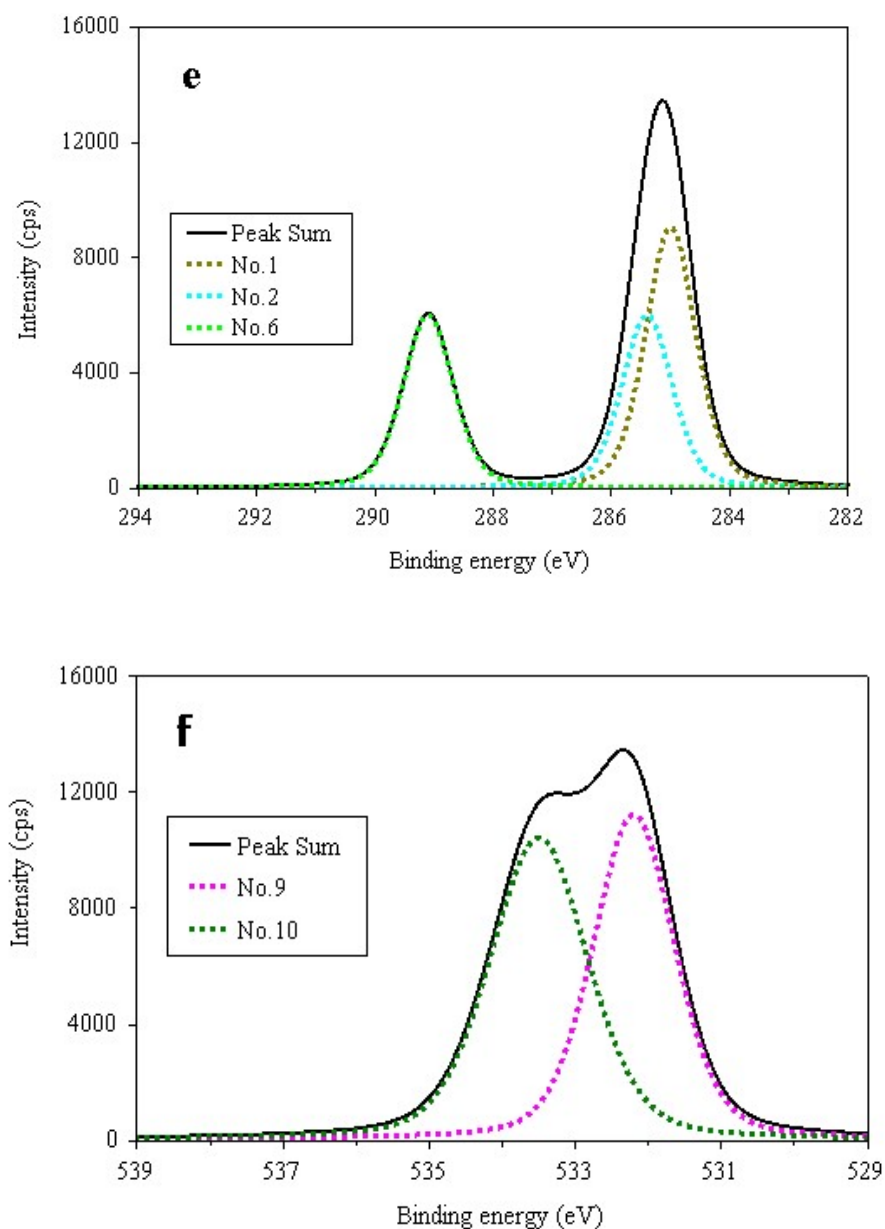


Fig. 2.6. High resolution XPS spectra of C1s (e) and O1s (f) of PVDF-g-PAA membrane (treatment: 20% (v/v) AA, 70°C, 30 min). The peak numbers in these figures corresponds to the Peak No. of Table 2.2.

Table 2.2 summarizes the BEs and functional groups from the results of high resolution XPS analysis.

Table 2.2

Summary of high resolution XPS scan results for untreated PVDF membrane, PVDF membrane treated with argon plasma (treatment: \pm 4.0 kVp-p, 180 s) and PVDF-g-PAA membrane (treatment: 20% (v/v) AA, 70°C, 30 min). When it is considered that some functional groups are included in each peak, these groups are identified by a number. Values represent the percentage associated to each or sum of bond type. Note that (-) denotes 0%. The underlined C or O means the objective carbon or oxygen.

Peak No.	BEs [eV]	Functional groups	Untreated PVDF	Plasma-treated PVDF	PVDF-g-PAA
1	285.0	-CH(COOH)- <u>CH</u> ₂ -CH(COOH)-	-	-	43.0
2	285.4	> <u>CH</u> -COOH	-	-	28.5
3	286.4	(1) -CF ₂ - <u>CH</u> ₂ -CF ₂ - (2) -CH ₂ - <u>CF</u> =CH- (3) -CH ₂ - <u>CF</u> =CH ₂ (4) -CH ₂ - <u>CH</u> (-OOH)-CH ₂ -	(1) 48.7	(1,2,3,4) 49.2	-
4	287.4	-CF ₂ - <u>CH</u> (-OOH)-CF ₂ -	-	16.7	-
5	288.5	(1) -CF ₂ - <u>CH</u> O (2) -CH ₂ - <u>CF</u> H-CH ₂ -	-	(1,2) 13.5	-
6	289.1	> <u>CH</u> - <u>CO</u> OH	-	-	28.5
7	289.5	-CH ₂ - <u>CF</u> (-OOH)-CH ₂ -	-	3.2	-

Peak No.	BEs [eV]	Functional groups	Untreated PVDF	Plasma-treated PVDF	PVDF-g-PAA
8	290.9	(1) -CH ₂ -CF ₂ -CH ₂ - (2) -CH ₂ -CFO (3) -CH=CF ₂	(1) 51.3	(1,2,3) 17.5	-
9	532.2	(1) >CH-COOH (2) -CH ₂ -CFO (3) -CF ₂ -CHO	-	(2,3) 2.8	(1) 47.4
10	533.5	(1) >CH-COOH (2) -CH ₂ -CF(-OOH)-CH ₂ - (3) -CF ₂ -CH(-OOH)-CF ₂ -	-	(2,3) 23.6	(1) 52.6
11	534.0	>C=OOH	-	73.6	-

The C1s high resolution spectrum of untreated PVDF membrane surface assigned to two distinct peaks at BEs of 286.4 eV due to $\text{CF}_2\text{-}\underline{\text{C}}\text{H}_2\text{-CF}_2$: No. 3 and 290.9 eV due to $\text{CH}_2\text{-}\underline{\text{C}}\text{F}_2\text{-CH}_2$: No. 8. Plasma-treated PVDF membrane and PVDF-g-PAA membrane showed complex C1s spectra. The underlined C or O in these linkages means the objective carbon or oxygen, and each number of decomposed peaks corresponds with peak number in Table 2.2.

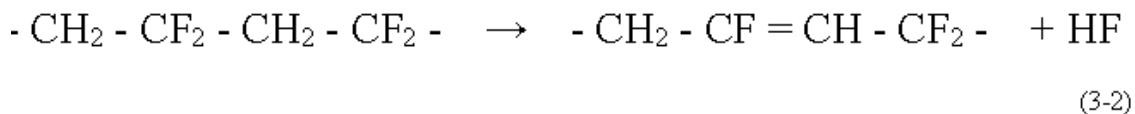
The C1s high resolution spectrum of plasma-treated PVDF membrane was decomposed into five peaks as shown in Table 2.2. The five peaks appeared at BEs of 286.4, 287.4, 288.5, 289.5 and 290.9 eV, which were assigned to $\text{CF}_2\text{-}\underline{\text{C}}\text{H}_2\text{-CF}_2$, $\text{CH}_2\text{-}\underline{\text{C}}\text{F}=\text{CH}$, $\text{CH}_2\text{-}\underline{\text{C}}\text{F}=\text{CH}_2$ and hydroperoxide ($\text{CH}_2\text{-}\underline{\text{C}}\text{H}(\text{-OOH})\text{-CH}_2$) groups (No. 3) ; hydroperoxide ($\text{CF}_2\text{-}\underline{\text{C}}\text{H}(\text{-OOH})\text{-CF}_2$) (No. 4); carbonyl ($\text{CF}_2\text{-}\underline{\text{C}}\text{HO}$) and $\text{CH}_2\text{-}\underline{\text{C}}\text{FH}\text{-CH}_2$ groups (No. 5); hydroperoxide ($\text{CH}_2\text{-}\underline{\text{C}}\text{F}(\text{-OOH})\text{-CH}_2$) (No. 7); and $\text{CH}_2\text{-}\underline{\text{C}}\text{F}_2\text{-CH}_2$ and carbonyl ($\text{CH}_2\text{-}\underline{\text{C}}\text{FO}$) and $\text{CH}=\underline{\text{C}}\text{F}_2$ groups (No. 8), respectively. The composition in Fig. 2.6(c) indicates surely that CF_2 carbons were modified into $\underline{\text{C}}\text{FH}$, $\underline{\text{C}}(\text{-OOH})$ and $\underline{\text{C}}\text{FO}$ carbons in the plasma exposure. On the other hand, the C1s high resolution spectrum of PVDF-g-PAA membrane was decomposed into characteristic three peaks attributable to AA graft polymerization. The three peaks observed at BEs 285.0, 285.4, and 289.1eV, which were individually assigned to $\text{-CH}(\text{COOH})\text{-}\underline{\text{C}}\text{H}_2\text{-CH}(\text{COOH})\text{-}$ (No. 1); $\underline{\text{C}}\text{H}\text{-COOH}$ (No. 2); and carboxy ($\text{CH}\text{-}\underline{\text{C}}\text{OOH}$) group (No. 6).

Likewise, the O1s high resolution spectrum of plasma-treated PVDF membrane was curve-fitted with three peaks at BEs of 532.2 eV for carbonyl ($\text{CH}_2\text{-CF}\underline{\text{O}}$) and aldehyde ($\text{CF}_2\text{-CH}\underline{\text{O}}$) groups (No. 9), 533.5 eV for hydroperoxide ($\text{CH}_2\text{-CF}(\text{-}\underline{\text{OOH}})\text{-CH}_2$, $\text{CF}_2\text{-CH}(\text{-}\underline{\text{OOH}})\text{-CF}_2$) groups (No. 10) and 534.0 eV for hydroperoxide ($\text{C-OO}\underline{\text{H}}$: No. 11) . On the other hand, the O1s high resolution spectrum of PVDF-g-PAA membrane was integrated with typical two peaks at BEs of 532.2 eV for carboxy group ($\text{CH-COO}\underline{\text{H}}$: No. 9) and 533.5 eV for carboxy group ($\text{CH-COO}\underline{\text{H}}$: No. 10).

2.3.5 The activation mechanism for initiation of graft polymerization

I attempted to elucidate the activation mechanism for PVDF membrane surface occurred by argon plasma treatment. Since the metastable argon, which is the most important active species in the present plasma, has an energy level of 11.5 eV [26], the energy transfer from metastable argon to the collided atom results in the link cleavage. The effect is comparable to the vacuum UV irradiation [27]. The following reactions for (i) dehydrofluorination, (ii) defluorination and (iii) dehydrogenation were inferred from the results of high resolution XPS scan shown in Table 2.2. The combination number after every equation corresponds to the numbers of peak and functional groups shown in Table 2.2, which means the resultant structure. For example, (3-2) shows the functional group (2) in peak No. 3, and (7) is consistent with the functional group of peak No. 7.

(i) A possible reaction of dehydrofluorination originated from plasma treatment is shown below.



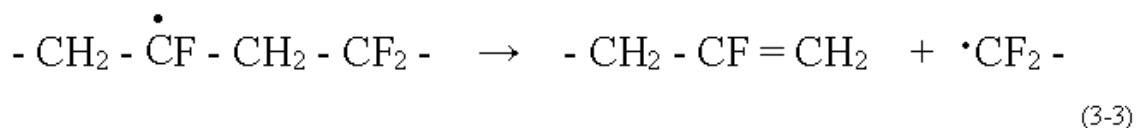
(ii) A possible reaction of defluorination occurred by plasma treatment is shown below.



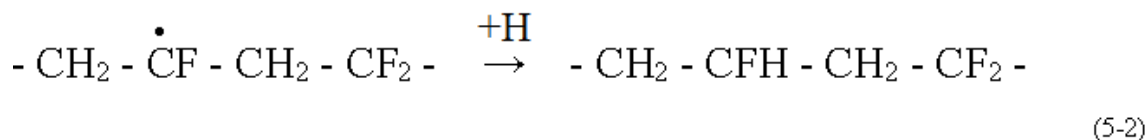
As a subsequent reaction, the distinct pathways would be considered.

1) The resulting radical leads to β -scission to yield the chain $-\text{CF}=\text{CH}_2$ double bond.

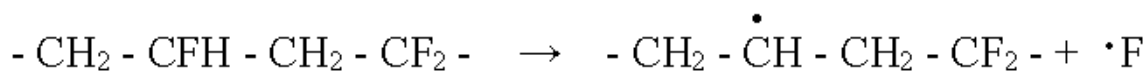
However, it is assumed to the underlined carbon atom of $-\text{CF}=\underline{\text{C}}\text{H}_2$ is negligible owing to the result of Table 2.2.



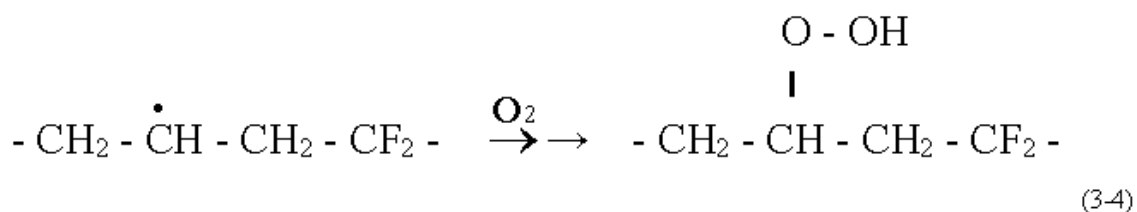
2) The resulting radical abstracts hydrogen from another polymer molecule.



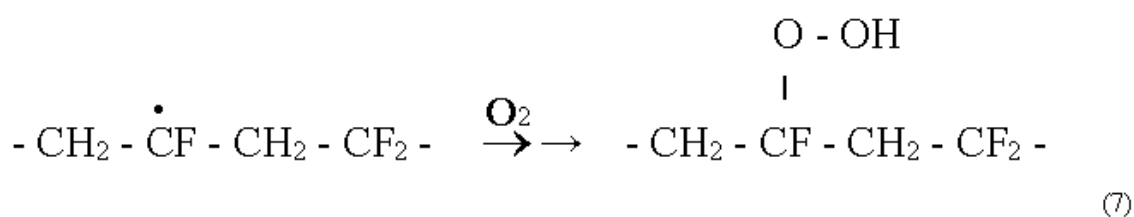
Following the reaction of 2), it is also possible that the remaining fluorine atom bound to the defluorinated carbon atom is eliminated with successive plasma treatment.



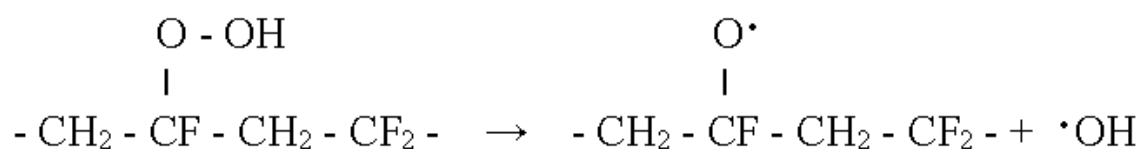
The resulting radical formed hydroperoxide group through oxidation. This pathway would progress to a small degree if the functional group (1) in peak No. 3 mostly remained.



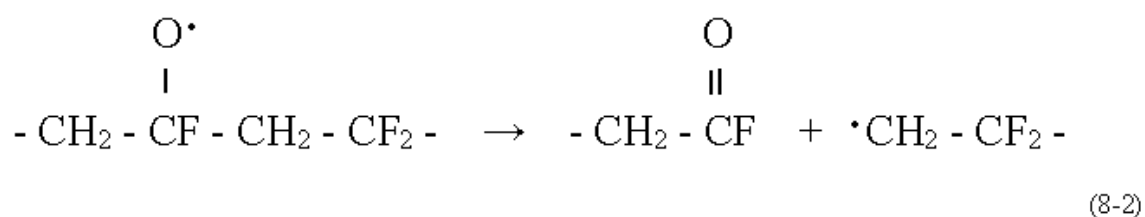
3) The resulting radical formed hydroperoxide group through oxidation.



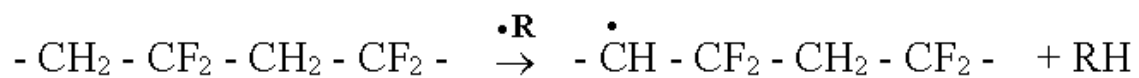
If the cleavage of single bond in hydroperoxide group progresses, it occurs oxyl radical and hydroxyl radical as shown.



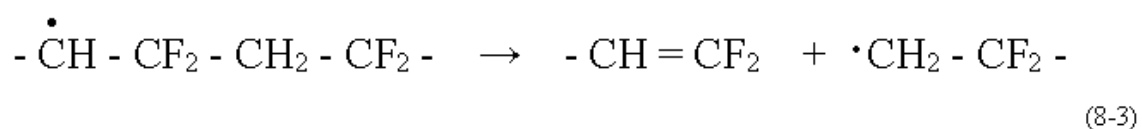
Afterwards, the oxyl radical would suffer β -scission immediately to yield the chain -CFO.



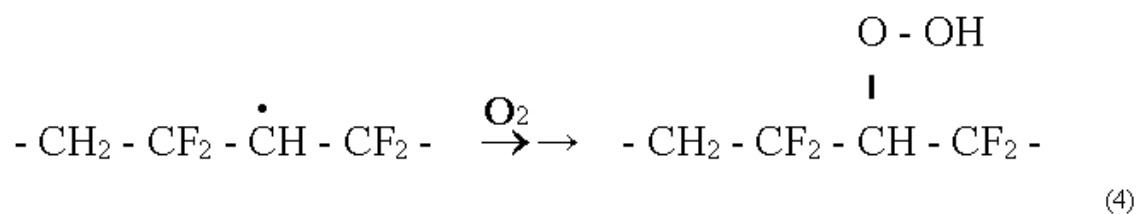
(iii) A possible mechanism of dehydrogenation originated from plasma treatment is shown below.



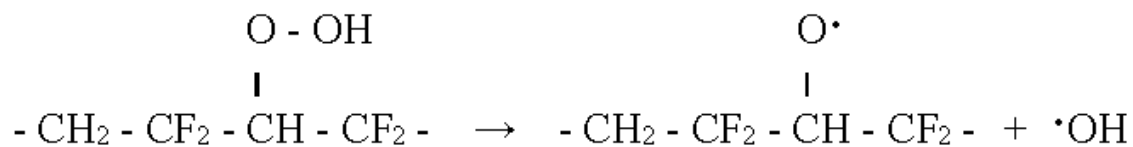
1) The resulting radical leads to β -scission to yield the chain $-\text{CH}=\text{CF}_2$ double bond.



2) The resulting radical formed hydroperoxide group through oxidation.



Likewise, if the cleavage of single bond in hydroperoxide group progresses, it occurs oxyl radical and hydroxyl radical as shown.



Afterwards, the oxyl radical would suffer β -scission immediately to yield the chain -CHO.

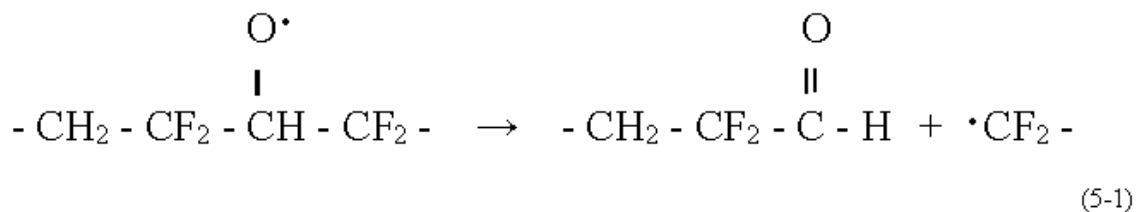


Table 2.2 shows that several hydroperoxide groups were produced on PVDF membrane treated with argon plasma. Therefore, I propose that hydroperoxide groups distributed on PVDF membrane treated with argon plasma were cleaved by thermal treatment, and originated some radicals induced to initiate graft polymerization.

2.3.6 Dependence of the degree of BSA conjugation on reaction conditions

Table 2.3 summarizes the atomic composition and the ratio of untreated PVDF, PVDF treated with argon plasma, PVDF-g-PAA and PVDF-g-PAA-BSA membranes. Nitrogen was also a target element monitored for two reasons. Firstly, PVDF is not constituted with nitrogen of the polymer elemental composition. Secondly, BSA is an approximately molecular weight 66 kDa protein contained nitrogen derived from its polypeptide backbone.

Table 2.3

Summary of atomic composition about untreated PVDF membrane, PVDF membrane treated with argon plasma (treatment: ± 4.0 kVp-p, 180 s), PVDF-g-PAA membrane (treatment: 20% (v/v) AA, 70°C, 30 min) and PVDF-g-PAA-BSA membrane (treatment: 1.00 mg mL⁻¹ BSA, 3.0 h) measured by XPS. Note that (-) denotes 0.

Membranes	Atomic composition				Atomic ratio	
	[%]				F/C	O/C
	F	C	O	N		
untreated PVDF	50.0	49.7	0.3	-	1.01	0.01
Argon plasma-treated PVDF	23.8	62.9	12.5	0.8	0.38	0.20
PVDF-g-PAA	-	65.8	34.0	0.1	-	0.52
PVDF-g-PAA-BSA	5.3	64.1	27.1	3.6	0.08	0.42

It can be seen that a small amount of nitrogen moieties is incorporated after plasma treatment and subsequent exposure to air. After grafting AA onto plasma-treated PVDF membrane, atomic nitrogen percentage decreased as low as 0.1%. After covalently immobilizing BSA onto PVDF-g-PAA membranes, atomic nitrogen percentage increased as high as 3.6%. However, fluorine was detected again onto PVDF-g-PAA-BSA membrane. As a source of the phenomenon, it was assumed that the PAA-ungrafted sites on PVDF-g-PAA-BSA membrane surface were revealed, because the conformation of PAA grafted onto PVDF-g-PAA membrane had been changed due to the conjugation with BSA.

Fig. 2.7 shows that changes in the nitrogen content of untreated PVDF membrane, PVDF-g-PAA membrane, PVDF-g-PAA membrane provided a semi-stable Sulfo-NHS ester (PVDF-g-PAA-NHS) and PVDF-g-PAA-BSA membranes fabricated using a different BSA solution of 0.04, 0.20 and 1.00 mg mL⁻¹.

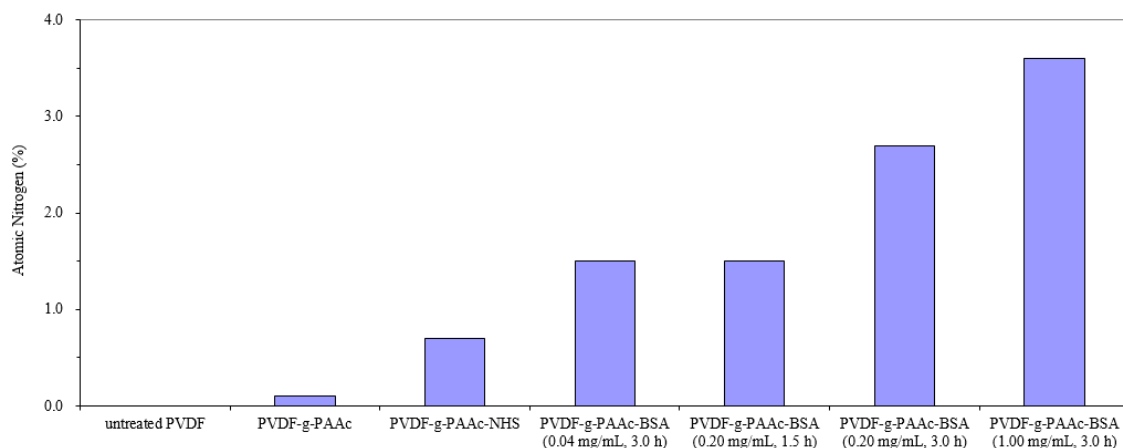


Fig. 2.7. XPS analysis of N1s levels for untreated PVDF membrane, PVDF-g-PAA membrane (treatment: 20% (v/v) AA, 70°C, 30 min), PVDF-g-PAA membrane provided a semi-stable Sulfo-NHS ester (PVDF-g-PAA-NHS), and conjugated PVDF-g-PAA-BSA (treatment: 1.00 mg mL⁻¹ BSA, 3.0 h). Nitrogen levels are elevated in PVDF-g-PAA-NHS due to the nitrogen in NHS. Conjugated BSA (as measured in terms of N content) increased with increasing BSA concentration in the conjugation solution and treatment time in case of 0.20 mg mL⁻¹.

Activated PVDF-g-PAA-NHS membrane showed 0.7% of nitrogen level, which is derived from the Sulfo-NHS. In order to investigate the effect of BSA concentration in the conjugation solution on the amount of nitrogen present, three different BSA concentrations were tested for 3.0 h as a fixed conjugation time. As shown in the Fig. 2.7, the nitrogen content increased significantly, suggesting that the conjugation reaction was concentration dependent. Likewise, in order to examine the relation between conjugation time and degree of BSA conjugation, I also conducted conjugation reactions for 1.5 h and 3.0 h using 0.20 mg mL⁻¹ BSA solution. As can be seen, the nitrogen content increased successfully from 1.5% to 2.7%. Another finding is that the nitrogen content was the same for both BSA conjugation treatments at 0.04 mg mL⁻¹ for 3.0 h and at 0.20 mg mL⁻¹ for 1.5 h. Taken together, these results demonstrate that alterations of protein concentration and treatment time potentially contribute to protein immobilization.

2.3.7 Membrane morphology

The 3-D scaffolds of membranes in this work are intended for biotechnology application in order to maintain the area capable of interacting with the objective, so it is important that plasma treatment and subsequent AA grafting reactions minimize the interference with their porosity. Thus, SEM images at magnification of 3000 \times for these membranes were taken before and after various chemical treatments in order to verify the impact on the porous structures and shown in Fig. 2.8. These membranes were treated with plasma from the above the upper surface.

In the features on the upper surface, the porous membrane fibers of the scaffolds for argon plasma treatment as shown in Fig. 2.8d had grown slightly thicker and the macrovoids formation was more uniform compared to untreated PVDF membrane surface as seen in Fig. 2.8a. However, PVDF-g-PAA membrane surface was densely modified with PAA as observed in Fig. 2.8g.

Likewise, in the appearance on the bottom surface, the membrane porosity after argon plasma treatment shown in Fig. 2.8e maintained the network structure of the untreated PVDF membrane surface represented by Fig. 2.8b. On the other hand, PVDF-g-PAA membrane surface shown in Fig. 2.8h was also grafted with PAA gentler than the upper surface of PVDF-g-PAA membrane as seen in Fig. 2.8g. Therefore, for sustaining the high porosity of the upper surface, it would be preferable to treat with the intensity of plasma equivalent to be present against the bottom surface, but in that case, conjugation level of BSA on the upper surface might be decreased.

The cross sectional view of PVDF-g-PAA membrane indicated in Fig. 2.8i showed that the PAA was grafted onto the upper and pore surfaces within the bulk of the membrane. To investigate the degree of distribution structured by graft polymerization of AA, I noted the cross sectional image of PVDF-g-PAA membrane at a magnification of 750 \times as shown in Fig. 2.8j. As the result of that, it was observed that each part described red and green arrows in the upper and bottom layer membrane of Fig. 2.8j respectively was uniformly grafted with PAA, and then these individual depths were approximately 37 μm and 13 μm . Thus, as for PVDF-g-PAA membrane, the graft yield in the upper of the membrane was expected to be approximately three times higher than in the bottom of that.

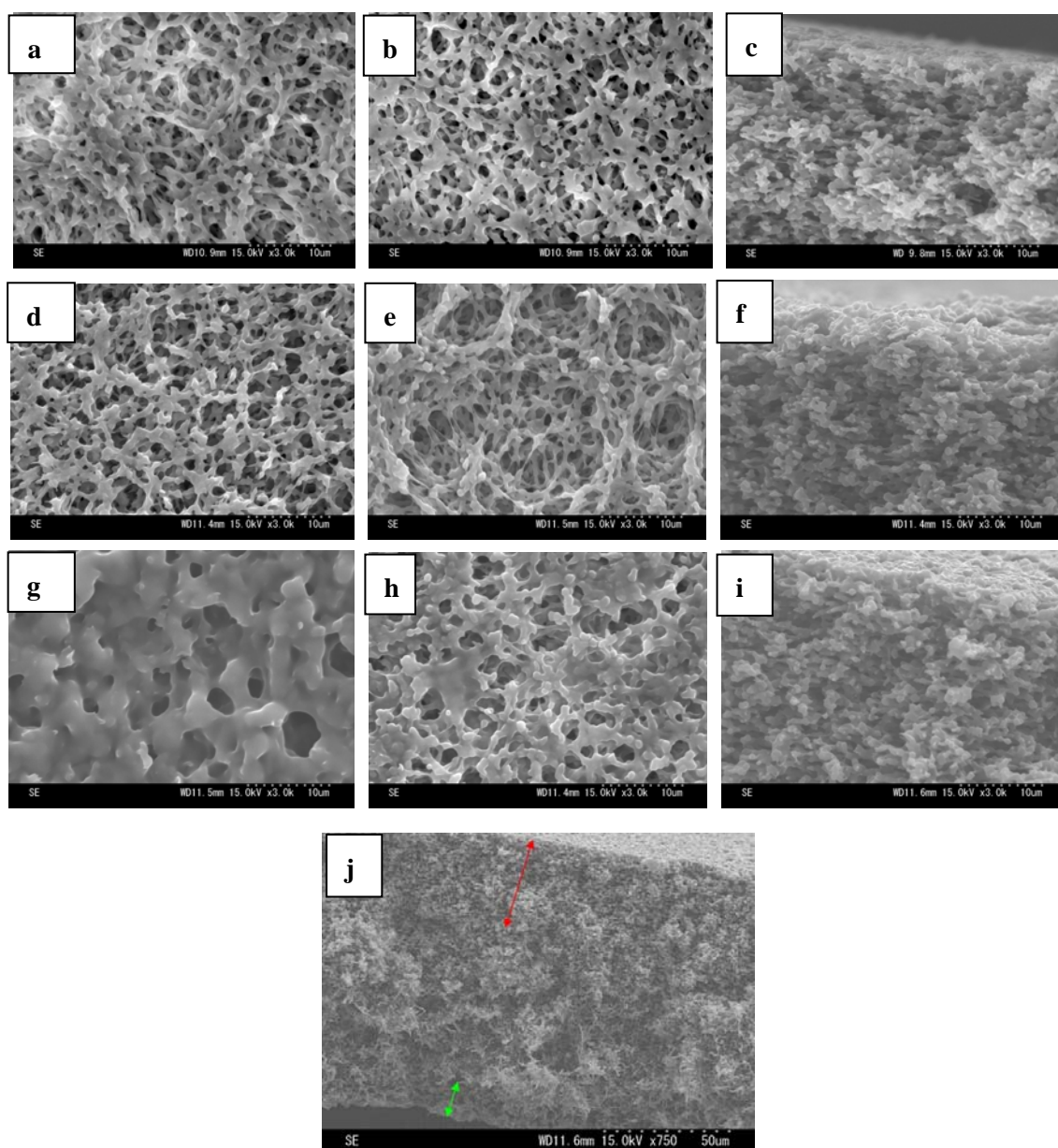


Fig. 2.8. SEM micrographs of untreated PVDF membrane (a, b, c), PVDF membrane treated with argon plasma (d, e, f; treatment: ± 4.0 kVp-p, 180 s), and PVDF-g-PAA membrane (g, h, i, j; treatment: 20% (v/v) AA, 70°C, 30 min). a, d, g: upper surface; b, e, h: bottom surface and c, f, i, j: cross section. These membranes were treated with argon plasma from the above of upper surface.

The cross sectional view of the PVDF-g-PAA membrane was also measured by SEM-EDX. These results show in Fig. 2.9. They were estimated that the PAA was densely grafted onto the upper of the membrane and the inside was with comparative uniform.

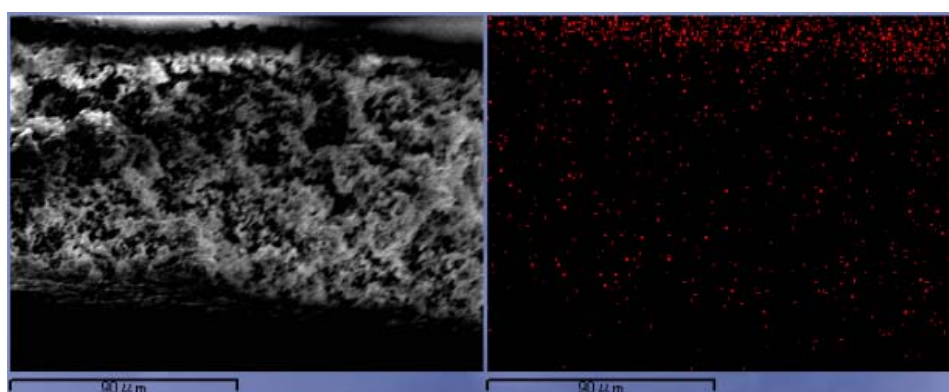


Fig. 2.9. SEM-EDX micrographs of the cross sectional PVDF-g-PAA membrane (magnification: 700×). Left: control, Right: the distribution profile of potassium atom. The membrane was treated with argon plasma from the above of upper surface.

AFM operating in dynamic force mode was performed to study the surface topography of untreated PVDF, plasma-treated PVDF and PVDF-g-PAA membrane. Table 2.4 reveals the surface roughness (R_a) of these membrane surfaces. The R_a was estimated from the AFM images on $5\ \mu\text{m}\times 5\ \mu\text{m}$ lateral area.

Table 2.4

Surface roughness of untreated PVDF membrane, PVDF membrane treated with argon plasma (treatment: $\pm 4.0\ \text{kVp-p}$, 180 s) and PVDF-g-PAA membrane (treatment: 20% (v/v) AA, 70°C , 30 min). The R_a was estimated from the AFM images on $5\ \mu\text{m}\times 5\ \mu\text{m}$ lateral area.

Membranes	Calculated average roughness (R_a) [nm]
Untreated PVDF	49.8
Argon plasma-treated PVDF	46.6
PVDF-g-PAA	5.9

Fig. 2.10 presents typical AFM images. From the results of Table 2.4, the R_a of argon plasma-treated PVDF membrane surface (46.6 nm; Fig. 2.10b) was a little decreased against that of untreated PVDF membrane surface (49.8 nm; Fig. 2.10a). The findings implied that the plasma condition for introducing functional groups was mild treatment against the membrane surface. On the other hand, I observed that there was shape like a high-density bumpy surface as shown in the AFM image on 500 nm×500 nm lateral area (Fig. 2.10e, 2.10h). These topological changes could result from chemical reactions and sputter processes of the plasma species with the surface. The observed features were also presumed to be a consequence of melting or recrystallization processes [28]. Hence, I am convinced that the plasma treatment is capable of modifying chemical and topological changes on the membrane surface simultaneously. Furthermore, the R_a of PVDF-g-PAA membrane (5.9 nm; Fig. 2.10c) was smooth and uniform structural features compared to plasma-treated PVDF membrane surface (46.6 nm; Fig. 2.10b).

As it has been also observed by R. Morent *et al.*, the surface morphology of the plasma deposited films (deposition time = 90 s) for the different discharge regions clearly showed that the surfaces of the plasma deposited polyacrylic acid membranes are quite smooth and that no significant differences in surface morphology can be found between the different discharge regions [29].

Taken together, I conclude that the plasma treatment is an excellent method to activate surface polymer of PVDF membrane, and plays an important role as pretreatment in fabricating chemically and physically uniform polymerized AA membrane.

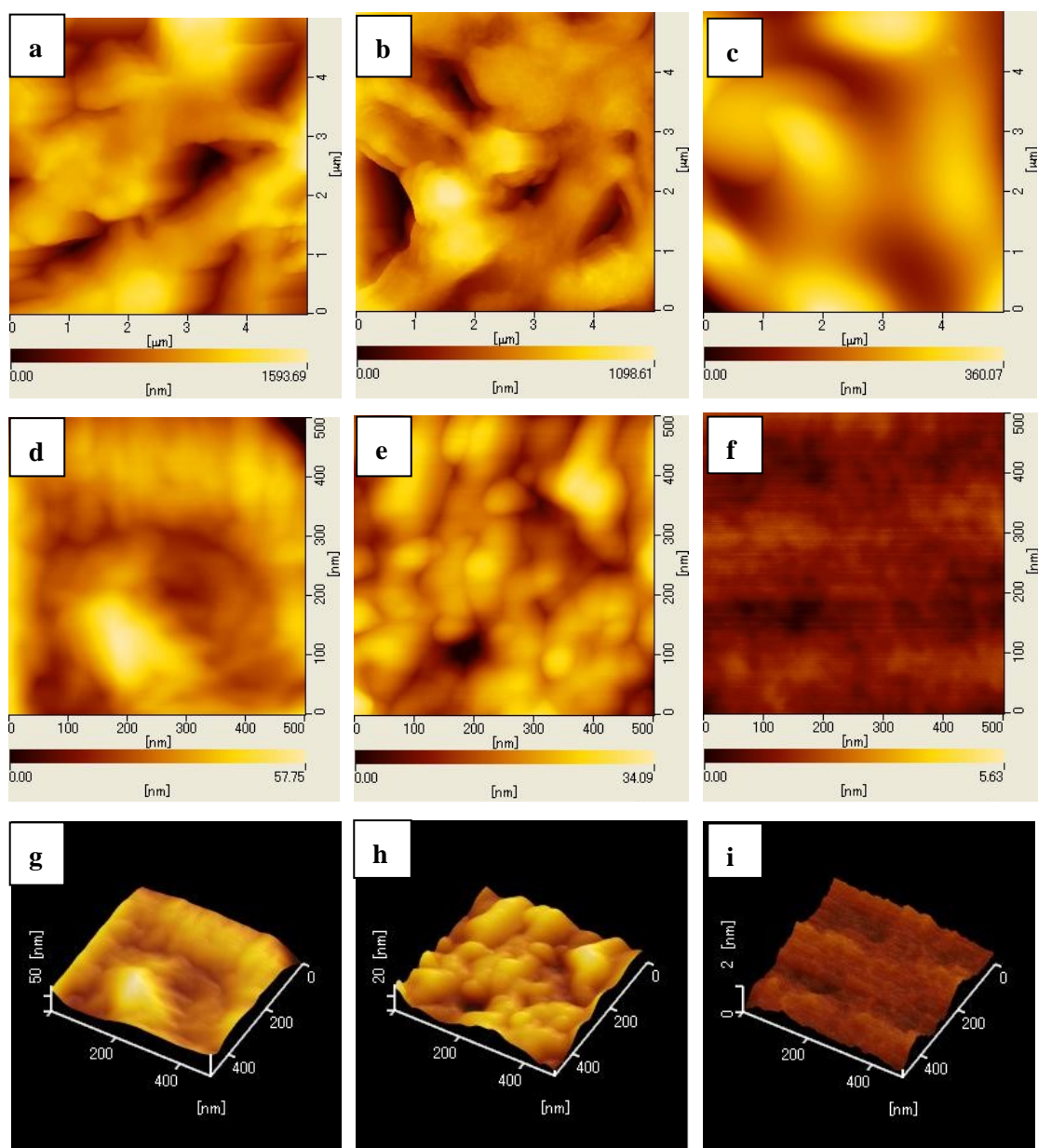


Fig. 2.10. Surface AFM images of untreated PVDF membrane (a, d, g), PVDF membrane treated with argon plasma (b, e, h; treatment: ± 4.0 kVp-p, 180 s) and PVDF-g-PAA membrane (c, f, i; treatment: 20% (v/v) AA, 70°C, 30 min). a, b, c: 5 $\mu\text{m} \times 5 \mu\text{m}$ lateral area; d, e, f, g, h, i: 0.5 $\mu\text{m} \times 0.5 \mu\text{m}$ lateral area.

2.4 Conclusions

In this work, the synthetic way to graft acrylic acid polymer on PVDF membrane surface using the CAPPLAT have been described. I attempted to elucidate the activation mechanism for PVDF membrane surface occurred by argon plasma treatment. The following reactions for dehydrofluorination, defluorination and dehydrogenation were inferred from the results of high resolution XPS scan. As the results, the initiator of graft polymerization is mainly hydroperoxide. Thus, it was proposed that these hydroperoxide groups were cleaved by thermal treatment, and originated some radicals induced to initiate graft polymerization. The porosity of the membrane scaffold was preserved after the plasma treatment. BSA was successfully conjugated on the polymer-modified PVDF membranes. The presence of BSA on the membranes was studied using high resolution XPS.

References

- [1] Liu Fu, Awanis Hashim N, Liu Yutie, Moghareh Abed MR, Li K. Progress in the production and modification of PVDF membranes. *J Membr Sci* 2011; 375:1.
- [2] Park YW, Inagaki N. Surface modification of poly (vinylidene fluoride) film by remote Ar, H₂, and O₂ plasmas. *Polymer* 2003; 44:1569.
- [3] Chu PK, Chen JY, Wang LP, Huang N. Plasma-surface modification of biomaterials. *Mater Sci Eng* 2002; 36:143.
- [4] Pascu M, Nicolas D, Poncin-Epaillard F, Vasile C. Surface modification of PVDF by plasma treatment for electroless metallization. *J Optoelectron Adv Mater* 2006; 8:1062.
- [5] Duca Mariana D, Plosceanu Carmina L, Pop Tatiana. Surface modifications of polyvinylidene fluoride (PVDF) under rf Ar plasma. *Polym Degrad Stab* 1998; 61:65.
- [6] Muller M, Oehr C. Plasma aminofunctionalisation of PVDF microfiltration membranes. *Surf Coatings Technol* 1999; 116-119:802.
- [7] Oehr Christian. Plasma surface modification of polymers for biomedical use. *Nucl Instr Meth Phys Res B* 2003; 208:40.
- [8] Mazzei Ruben, Smolko Eduardo, Tadey Daniel, Gizzi Laura. Radiation grafting of NIPAAm on PVDF nuclear track Membranes. *Nucl Instr Meth Phys Res B* 2000; 170:419.
- [9] Forsythe JS, Hill DJT. The radiation chemistry of fluoropolymers. *Prog Polym Sci* 2000; 25:101.
- [10] Berthelot Thomas, Le Xuan Tuan, Jégou Pascale, Viel Pascal, Boizot Bruno, Baudin Cécile, *et al.* Photoactivated surface grafting from PVDF surfaces. *Appl Surf Sci*

2011; 257:9473.

[11] Lubarsky GV, Davidson MR, Bradley RH. Characterisation of polystyrene microspheres surface-modified using a novel UV-ozone/fluidised-bed reactor.

Appl Surf Sci 2004; 227:268.

[12] Deng Jianping, Wang Lifu, Liu Lianying, Yang Wantai. Developments and new applications of UV-induced surface graft polymerizations. Prog Polym Sci 2009; 34:156.

[13] Zhang Minggang, Nguyen Quang Trong, Ping Zhenghua. Hydrophilic modification of poly (vinylidene fluoride) microporous membrane. J Membr Sci

2009; 327:78.

[14] Chen Yiwang, Deng Qilan, Xiao Jichun, Nie Huarong, Wu Lichuan, Zhou Weihua, *et al.* Controlled grafting from poly (vinylidene fluoride) microfiltration membranes via reverse atom transfer radical polymerization and antifouling properties. Polymer 2007; 48:7604.

[15] He Dongming, Susanto Heru, Ulbricht Mathias. Photo-irradiation for preparation, modification and stimulation of polymeric membranes. Prog Polym Sci 2009; 34:62165.

[16] Yamago Shigeru, Nakamura Yasuyuki. Recent progress in the use of photoirradiation in living radical polymerization. Polymer 2013; 54:981.

[17] Tendero Claire, Tixier Christelle, Tristant Pascal, Desmaison Jean, Leprince Philippe. Atmospheric pressure plasmas: a review. Spectrochim Acta

Part B 2006; 61:2.

[18] Noeske Michael, Degenhardt Jost, Strudthoff Silke, Lommatzsch Uwe. Plasma jet treatment of five polymers at atmospheric pressure: surface modifications and the relevance for adhesion. Int J Adhesion Adhesives 2004; 24:171.

- [19] Merche Delphine, Vandencastele Nicolas, Reniers François. Atmospheric plasmas for thin film deposition: a critical review. *Thin Solid Films* 2012; 520: 4219.
- [20] Chen Mingsheng, Zhang Ying, Yao Xiaomei, Li Hao, Yu Qingsong, Wang Yong. Effect of a non-thermal, atmospheric-pressure, plasma brush on conversion of model self-etch adhesive formulations compared to conventional photopolymerization. *Dent Mater* 2012; 28:1232.
- [21] Gu Minghao, Kilduff James E, Belfort Georges. High throughput atmospheric pressure plasma-induced graft polymerization for identifying proteinresistant surfaces. *Biomaterials* 2012; 33:1261.
- [22] Kuwabara Atsushi, Kuroda Shin-ichi, Kubota Hitoshi. Development of atmospheric pressure plasma low temperature surface discharge plasma torch and application to polypropylene surface treatment. *Plasma Chem Plasma Process* 2008; 28:263.
- [23] Mizote Norihito, Kuroda Shin-ichi. Friction characteristics of amorphous carbon films on rubber deposited by cold atmospheric pressure plasma. *Tribol Online* 2012; 7:234.
- [24] Hidzir Norsyahidah Mohd, Hill David JT, Martin Darren, Grøndahl Lisbeth. Radiation-induced grafting of acrylic acid onto expanded poly (tetrafluoroethylene) membranes. *Polymer* 2012; 53:6063.
- [25] Liu Fu, Du Chun-Hui, Zhu Bao-Ku, Xu You-Yi. Surface immobilization of polymer brushes onto porous poly (vinylidene fluoride) membrane by electron beam to improve the hydrophilicity and fouling resistance. *Polymer* 2007; 48:2910.
- [26] W.L. Wiese, M.W. Smith and B.M. Miles. Atomic transition probabilities, NSRDS-NBS 22, Washington, DC, 1969.

[27] Matienzo LJ, Zimmerman JA, Egitto FD. Surface modification of fluoropolymers with vacuum ultraviolet irradiation. *J Vac Sci Technol A* 1994; 12:2662.

[28] Noeske Michael, Degenhardt Jost, Strudthoff Silke, Lommatzsch Uwe. Plasma jet treatment of five polymers at atmospheric pressure: surface modifications and the relevance for adhesion. *Int J Adhesion Adhesives* 2004; 24:171.

[29] Morent R, De Geyter N, Van Vlierberghe S, Beaurain A, Dubruel P, Payen E. Influence of operating parameters on plasma polymerization of acrylic acid in a mesh-to-plate dielectric barrier discharge. *Prog Org Coatings* 2011; 70:336.

Chapter 3 Preparation and characterization of Protein A-immobilized PVDF and PES membranes

3.1 Introduction

Fluoropolymers have excellent features, such as electrical and chemical resistance, high thermal stability and low surface energies [1]. Fluorinated polymers are applied in many industries, such as for thin film technology magnetic media, non-stick cookware and engineering plastics [2]. One of the commercially available fluoropolymers is PVDF. Research and application of PVDF membranes has been reported since the 1980s [3]. One of the reasons for this is that PVDF dissolves in common organic solvents, so porous PVDF membranes can be produced via phase inversion methods with a simple immersion precipitation process. On the other hand, polyether sulfone (PES) has also been widely available commercially, and has excellent mechanical strength and is a thermally stable polymer [4]. Thus, PES membranes have been adopted as important materials in the food, hemodialysis and water purification fields, as well as for biopharmaceutical drugs as MF and UF [5]. PES and PVDF membranes are valuable as research subjects in separation fields. However, PVDF and PES have the issue of being intrinsically and severely hydrophobic [6]. As the result, proteins dissolved in aqueous solutions tend to clog the membranes. Therefore, manufacturers provide membranes that are hydrophilized to decreasing the nonspecific protein binding capacity with various surface modifications to prevent objective substances, such as recombinant proteins, from fouling the membranes [7, 8]. Other advancements in the field have been related to pore size distributions and membrane types, which are critical factors to

achieve anti-fouling properties, and deal with variations at the production scale. High capacity membranes have been developed for the biotechnology industry with varying pore size distributions, such as isotropic and anisotropic structures [9].

In recent years, many functionalized membranes with surface modifications have been reported [10-12]. There has been significant interest in using affinity membrane chromatography for bioprocessing, but few reports are applied in production scales because the adsorption capacities of the affinity membranes are relatively low compared with those for conventional bead chromatography [13]. Humanized mAbs, which belong to a subclass of IgG, have been utilized in clinical fields as drug products [14]. To capture mAbs efficiently from the pool of the mAb production, Protein A is widely applied as a ligand on affinity chromatography media because Protein A strongly binds on the Fc region of IgG [15]. However, native Protein A originates from *Staphylococcus aureus* [9]. Therefore, it is important to establish a method for immobilizing Protein A on the media because of the decrease in the amount of leached Protein A. Simultaneously, a media with good chemical resistance and thermally stable features should be selected. As such, PVDF and PES membranes are important candidates as affinity media.

Plasma processing is a dry process for clean and energy saving surface modifications [16, 17]. Compared to plasma processing with a vacuum, atmospheric pressure low-temperature plasma does not need equipment for vacuum processing [18]. Plasma induced free radical polymerization is a useful technique for grafting polymers to hydrophilize or functionalize the surface of a polymeric substrate [19]. On the other

hand, surface modifications on hydrophilic PVDF membranes have also been reported to have a covalent coupling of lysine as model of biologically active molecules [20]. It is highly plausible to minimize nonspecific adsorption on the membrane because the protein adsorption capacity of hydrophobic and hydrophilic PVDF membranes varies significantly, reportedly from 1157 and 84 mg m⁻² [21].

The first goal of our study was to reveal the activation mechanism of PVDF and PES membranes activated by atmospheric pressure low-temperature plasma. The surface chemicals and morphological properties of the membranes were characterized by ATR FT-IR spectroscopic analysis, SEM and XPS. The second goal of our study was to characterize the properties of Protein A-immobilized PVDF and PES membranes. The adsorption capacities with human IgG were confirmed according to the monolayer Langmuir model [22], and the ligand density on the membranes was also measured using a BCA protein assay [23].

3.2 Experimental

The similar materials and methods as this chapter are referred to the chapter 2.

3.2.1 Materials

PVDF (Durapore[®], hydrophilic) membranes were purchased from Merck Millipore Corp., commercially named HVL01300 (pore size 0.45 μm) and SVLP01300 (pore size 5.0 μm). A PES membrane (Millipore Express[®] PLUS) was also purchased from Merck Millipore Corp., commercially named HPWP01300 (pore size 0.45 μm). Protein A from *Staphylococcus aureus* was purchased from Calbiochem (Darmstadt, Germany). IgG from human serums were purchased from Sigma-Aldrich, Inc. The Micro BCA protein assay kit was purchased from Thermo Fisher Scientific Inc.

3.2.2 Preparation of the PVDF and PES membranes immobilized with Protein A

Fig. 3.1 shows a schematic illustration of the preparation for the PVDF/PES membranes immobilized with Protein A. The PVDF and PES membranes grafted with PAA (hereafter called PVDF-g-PAA and PES-g-PAA, respectively or PVDF/PES-g-PAA) were rinsed with distilled water to remove non-grafted monomers. Protein A was immobilized on the PVDF/PES-g-PAA membranes using the EDC/Sulfo-NHS method. The membranes were activated with a 4 mmol L^{-1} EDC, 10 mmol L^{-1} Sulfo-NHS in 100 mmol L^{-1} MES, 500 mmol L^{-1} NaCl buffer solution with a pH of 6.0 for 15 min at room temperature. The immobilization of Protein A was carried out in a solution of 1 mg mL^{-1} Protein A in 100 mmol L^{-1} MES, 500 mmol L^{-1} NaCl buffer with a pH of 6.0

under mild agitation for 3.0 h at room temperature. The immobilization reaction of the PVDF and PES membranes (hereafter called PVDF-g-PAA-PrA and PES-g-PAA-PrA, respectively or PVDF/PES-g-PAA-PrA) was quenched by adding hydroxylamine HCl to give a final concentration of 10 mmol L⁻¹. The membranes were rinsed with a solution of PBS (-) to remove loosely absorbed Protein A and the MES buffer solution, and then kept in a solution of PBS (-) at 5°C.

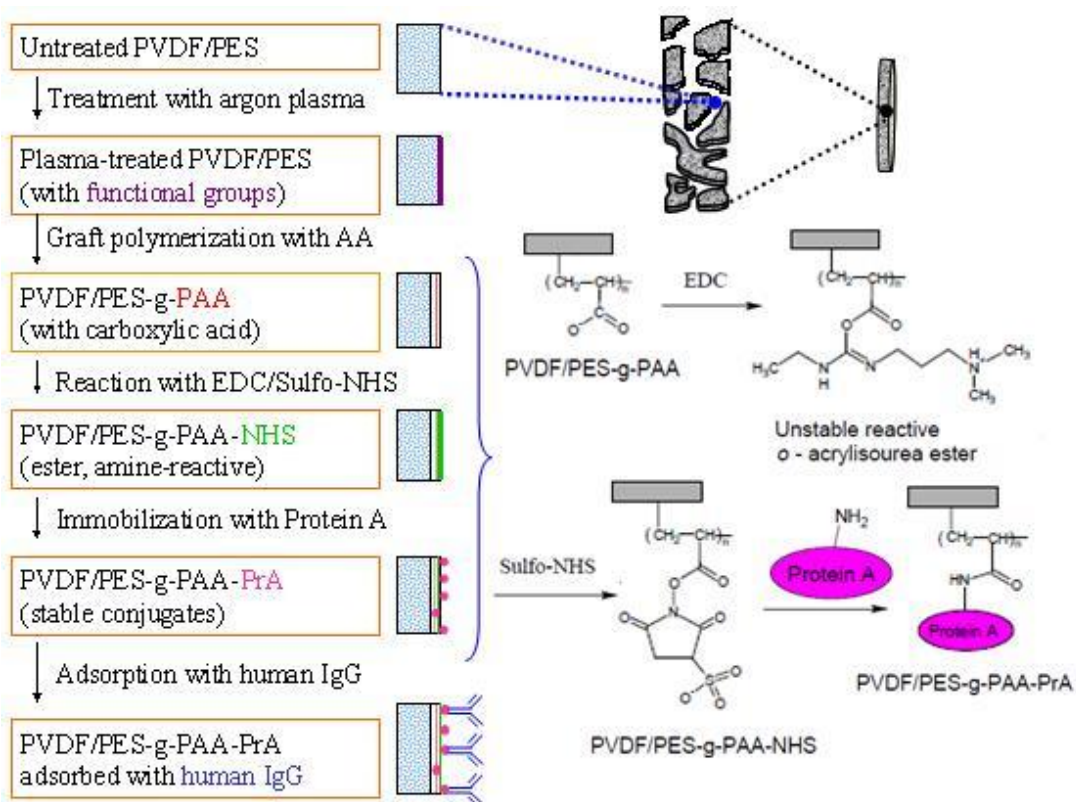


Fig. 3.1. Schematic illustration of the preparation for the PVDF and PES membranes immobilized with Protein A and the adsorption with human IgG.

3.2.3 Physical and chemical surface characterization

ATR FT-IR spectroscopic investigations were carried out with a Nicolet iS10 spectrometer using a Ge crystal. The spectra were collected by cumulating 64 scans at a resolution of 2 cm⁻¹.

3.2.4 Determination of adsorption capacities

The nonspecific adsorption on the PVDF/PES-g-PAA membranes and the adsorption isotherm on the PVDF/PES-g-PAA-PrA membranes with a human IgG were measured. Four of the membranes were employed in each closed glass vessel. The membranes were equilibrated in a solution of PBS (-) at a pH of 7.4 as an equilibrium buffer solution for 10 min. The equilibrium buffer solution was replaced with 4 mL of the equilibrium buffer solution dissolved with different concentrations of human IgG, and incubated for 12 h at 20°C. The amount of human IgG adsorbed on the membranes was determined by measuring the concentration of human IgG in the solution before and after the adsorption experiments were performed. Each concentration of human IgG was measured by a Micro BCA protein assay. The adsorption isotherms were constructed by plotting the adsorption capacity on the membranes versus the equilibrium concentration of human IgG dissolved in the liquid. Data were analyzed according to the monolayer Langmuir model shown in Equation (1).

$$q^* = \frac{q_m \cdot K_a \cdot c^*}{1 + K_a \cdot c^*} \quad (1)$$

where the c^* and q^* represented the equilibrium concentration of the human IgG dissolved in the liquid and the equilibrium capacity of human IgG adsorbed on the membranes, respectively. The variable q_m represented the maximum adsorption capacity on the membranes and K_a represented the equilibrium association constant. Equation (1) was transformed into a linear form as a double reciprocal plot, shown in Equation (2), to calculate q_m and K_a .

$$\frac{1}{q^*} = \frac{1}{q_m} + \frac{1}{K_a \cdot q_m} \cdot \frac{1}{c^*} \quad (2)$$

where the q^* and q_m were calculated in mg mL^{-1} , which represents the weight of human IgG adsorbed per volume of the membrane. Variable K_a was calculated in L mol^{-1} by considering the molecular weight to be 146 kDa [24].

3.2.5 Determination of ligand densities

The amount of Protein A covalently immobilized on each PVDF/PES-g-PAA-PrA membrane was measured with a BCA protein assay [13]. The ligand density was calculated in mg mL^{-1} , which represents the weight of Protein A immobilized per volume of the membrane.

3.2.6 Procedure of stability test

The PVDF/PES-g-PAA-PrA membranes were treated by repeating the cycle of equilibration, adsorption, elution, washing and regeneration to estimate the stability of the membranes. Four membranes were employed in each closed glass vessel. First, the membranes were equilibrated by a solution of PBS (-) at a pH of 7.4 as an equilibrium buffer solution for 10 min (equilibration), and then replaced in 4 mL of the equilibrium buffer solution dissolved 0.1 mg mL^{-1} human IgG for 10 min (adsorption). Secondly, the membranes were immersed in 4 mL of 0.1 mol L^{-1} citric acid buffer solution at a pH of 3.0 for 10 min (elution), and then washed with a solution of PBS (-) at a pH of 7.4 for 10 min (washing). Finally, the membranes were immersed in 20% (v/v) ethanol for 20 min (regeneration). After the five cycles were performed, the ligand densities of the membranes were measured.

3.3 Results and discussion

3.3.1 Structure characterization of the membranes by ATR-FTIR analysis

Fig. 3.2 shows the respective ATR-FTIR spectra of PES membrane and represented the data of the membranes untreated, treated with argon plasma, grafted with AA and those immobilized with the Protein A. The ATR-FTIR spectra of the PVDF membranes were similar to those in the previous report [19].

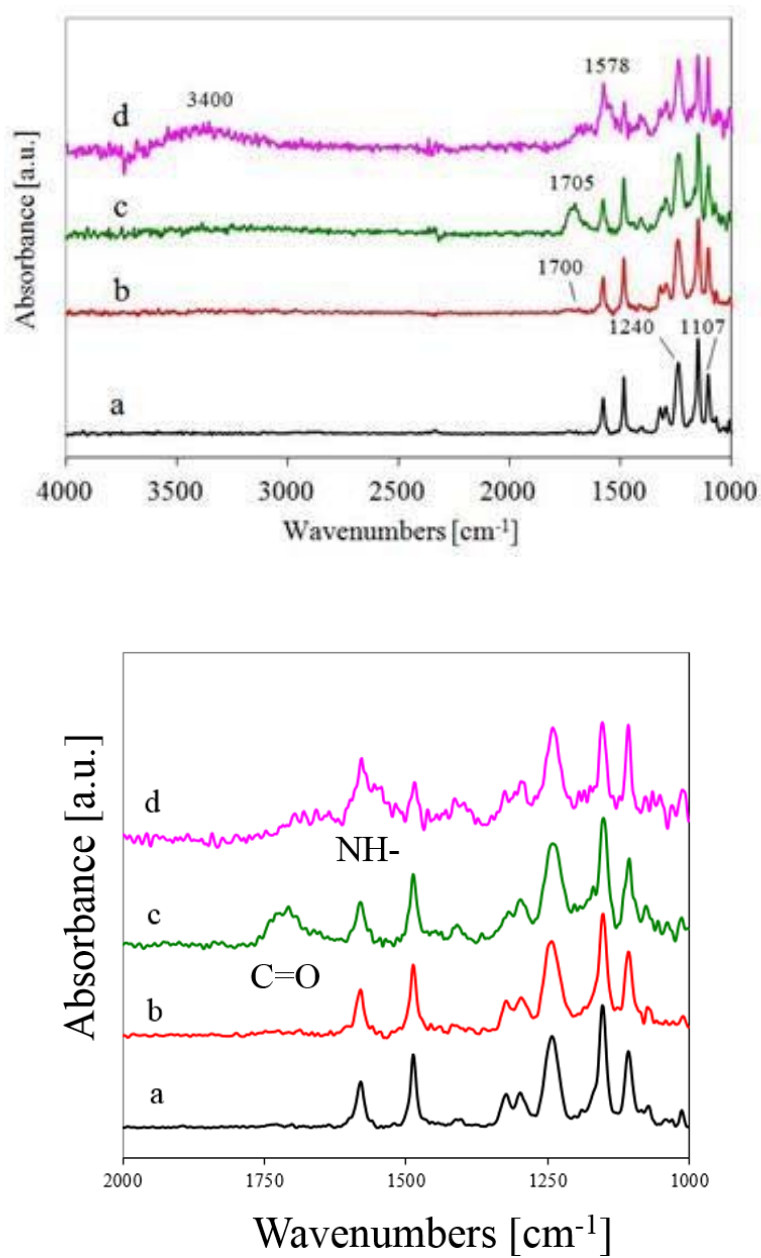


Fig. 3.2. ATR-FTIR spectra of PES membranes. (a) untreated, (b) treated with argon plasma (treatment: ± 4.0 kVp-p, 180 s), (c) grafted with AA (treatment: 20% (v/v) AA, 70°C, 20 min) and (d) immobilized with Protein A (treatment: 1 mg mL⁻¹, 3 h).

The strong absorption bands at 1107 - 1240 cm^{-1} were characteristic bands of aromatic ethers and sulfonyl groups of PES (Fig. 3.2a). The spectrum of the plasma-treated PES membrane contained a weak absorption band at approximately 1700 cm^{-1} (Fig. 3.2b). The spectrum of the PES-g-PAA membrane appeared with a strong carbonyl (C=O) stretching absorption band at 1705 cm^{-1} (Fig. 3.2c). This indicates that polyacrylic acid chains were successfully grafted on the membrane. The spectrum of the PES-g-PAA-PrA membrane revealed the increase of the absorption band attributed to the NH-deformation vibration at 1578 cm^{-1} , and broad absorption bands attributed to primary amino groups with a maximum at 3400 cm^{-1} were strongly observed (Fig. 3.2d). Consequently, it was demonstrated that Protein A was successfully immobilized on the PES-g-PAA membrane.

3.3.2 Structure characterization of the membranes by XPS analysis

I investigated the influence of defluorination and oxidation on the plasma treatment time and applied voltage compared with untreated PVDF membranes. The atomic composition was estimated from relative intensities of C1s, F1s, O1s, N1s and S2p high resolution spectra. Atomic ratios of the PVDF and PES samples are summarized in Tables 3.1 and 3.2, respectively.

Table 3.1.

Atomic ratios of the PVDF membrane (pore size 0.45 μm) surfaces exposed to argon plasma (treatment: flow rate of argon gas at 5 L min^{-1}).

Plasma treatment		Atomic ratio		Defluorination	Oxidation
Voltage	Exposure time	F/C	O/C	[%]	[%]
[\pm kVp-p]	[s]				
-	-	0.72	0.13	0	0
4.0	60	0.59	0.16	18	23
4.0	180	0.59	0.17	18	31
4.0	300	0.55	0.20	24	54
2.8	180	0.67	0.18	7	38
4.0	180	0.59	0.17	18	31
5.0	180	0.59	0.20	18	54

The F/C and O/C atom ratios of the untreated PVDF membrane were individually 0.72 and 0.13 due to the hydrophilic treatment from the manufacturer. In the case of the plasma-treated PVDF membranes, the defluorination reactions proceeded 18%, 18% and 24% for 60, 180 and 300 s of plasma exposure time, respectively. Secondly, the degree of defluorination resulted in 7%, 18% and 18% at ± 2.8 , ± 4.0 and ± 5.0 kVp-p, respectively. The sample treated at ± 5.0 kVp-p was appeared to have an intensively burnt area, so it was presumed to lead to heavy etching reactions. In a recent related report of the argon plasma treatment to other fluoropolymers, Hidzir *et al.* described that the chemical environment of the surface of expanded poly (tetrafluoroethylene), which was treated with 100 W argon plasma under the low pressure and subsequently exposed to air changed substantially, displayed evidence of defluorination (F/C atom ratio of 1.9 from 2.4) [25]. On the other hand, oxidation reactions progressed 23%, 31% and 54% for 60, 180 and 300 s, respectively, compared with an untreated PVDF membrane. Moreover, the degree of oxidation was 38%, 31% and 54% at ± 2.8 , ± 4.0 and ± 5.0 kVp-p. These data imply that the oxygen functional groups, such as peroxide species, were generated on the plasma-treated PVDF membrane.

Table 3.2.

Atomic ratios of the PES membrane surfaces exposed to argon plasma (treatment: flow rate of argon gas at 5 L min⁻¹).

Plasma treatment		Atomic ratio		Oxidation
Voltage	Exposure time	O/C	S/C	[%]
[± kVp-p]	[s]			
-	-	0.37	0.049	0
4.0	60	0.50	0.087	35
4.0	180	0.66	0.075	78
4.0	300	0.77	0.064	108
2.8	180	0.54	0.069	46
4.0	180	0.66	0.075	78
5.0	180	0.78	0.110	111

The O/C and S/C atom ratios of the untreated PES membrane were 0.37 and 0.049, respectively, due to the hydrophilic treatment. In the case of the plasma-treated PES membranes, the oxidation reactions proceeded 35%, 78% and 108% for 60, 180 and 300 s, respectively. Secondly, the degree of oxidation was 46%, 78% and 111% at ± 2.8 , ± 4.0 and ± 5.0 kVp-p, respectively. Moreover, the oxidation reaction on the PES membranes progressed approximately two times higher than that of the PVDF membranes. These findings suggest that the plasma-treated PES membrane has more initiation sites for graft polymerization relative to the plasma-treated PVDF membrane.

Fig. 3.3 shows C1s high resolution spectra for the untreated PVDF membrane and plasma-treated PVDF membrane. The decomposed peaks are illustrated as dotted lines. The underlined C, O or S means the objective was carbon, oxygen or sulfur, respectively.

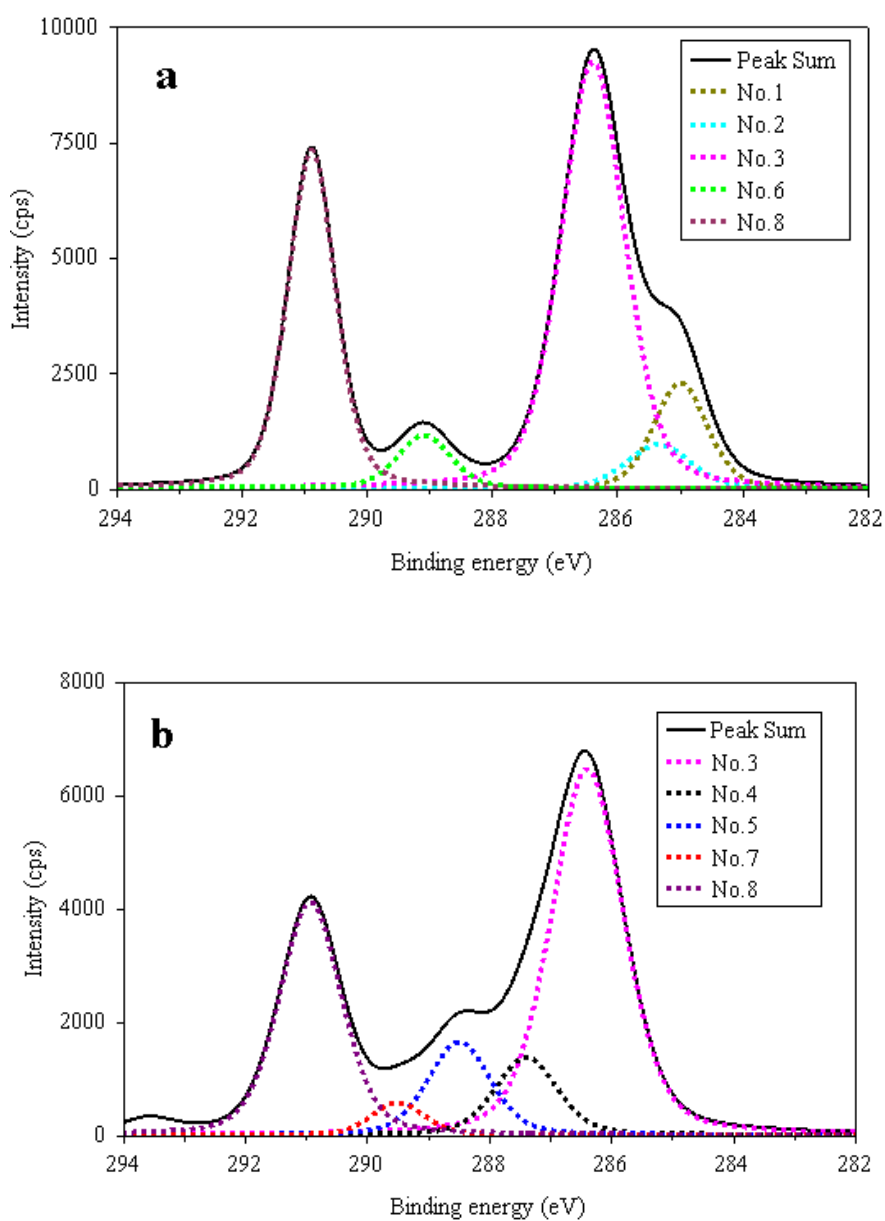


Fig. 3.3. High resolution XPS spectra of C1s. (a) untreated PVDF (pore size 0.45 μm) membrane and (b) PVDF membrane treated with argon plasma (treatment: ± 4.0 kVp-p, 180 s).

The C1s high resolution spectrum of the untreated PVDF membrane was assigned to five peaks at BEs of 285.0 eV due to CH(COOH)-CH₂-CH(COOH) : No. 1, 285.4 eV due to CH-COOH : No. 2, 286.4 eV due to CF₂-CH₂-CF₂ : No. 3, 289.1 eV due to CH-COOH : No. 6 and 290.9 eV due to CH₂-CF₂-CH₂ : No. 8 (Fig. 3.3a). These data indicate that the untreated PVDF membrane is cross-linked with hydroxyalkyl acrylate to hydrophilize the membrane [7]. The C1s high resolution spectrum of the plasma-treated PVDF membrane was decomposed into five peaks (Fig. 3.3b) [19]. The five peaks appeared at BEs of 286.4, 287.4, 288.5, 289.5 and 290.9 eV, which were assigned to CF₂-CH₂-CF₂, CH₂-CF=CH, CH₂-CF=CH₂ and hydroperoxide (CH₂-CH(-OOH)-CH₂) groups (No. 3); hydroperoxide (CF₂-CH(-OOH)-CF₂) (No. 4); carbonyl (CF₂-CHO) and CH₂-CFH-CH₂ groups (No. 5); hydroperoxide (CH₂-CF(-OOH)-CH₂) (No. 7); and CH₂-CF₂-CH₂ and carbonyl (CH₂-CF₂O) and CH=CF₂ groups (No. 8), respectively. The composition showed that CF₂ carbons were modified into CFH, C(-OOH) and CF₂O carbons in the plasma exposure. Lee and Shim have measured the concentration of peroxides formed on the argon plasma-treated PVDF membranes (pore size 0.22 μm and 70% porosity) by the 1,1-diphenyl-2-picrylhydrazyl (DPPH) method [26]. The density of peroxides showed 2.5×10^{-8} mol cm⁻² at 30 W for 30 s in 50 mTorr. Although the density increased until the 30 s exposure, interestingly, it decreased with a 40 s exposure. These data suggested that the C1s high resolution spectrum shape of the plasma-treated PVDF membrane as shown in Fig. 3.3 was dependent on the exposure conditions.

The C1s high resolution spectrum of the PVDF-g-PAA membrane was decomposed into three characteristic peaks attributable to the AA graft polymerization. The three peaks

observed at BEs of 285.0, 285.4 and 289.1 eV, were individually assigned to the CH(COOH)-CH₂-CH(COOH); CH-COOH; and carboxy (CH-COOH) groups.

Graft polymerization of acrylic acid is a useful method for forming many carboxy groups on the membranes to react with EDC, and subsequently results in a semi-stable amine-reactive NHS ester. In addition, Huang *et al.* have reported that plasma induced grafting of acrylic acid significantly improved the wettability behavior of the PVDF nanofiber membranes [27]. In this way, there are some advantages of applying the polymerization, but it is important to optimize the grafting conditions because excessive grafting leads to a decrease in the porosity and surface area of the microporous membranes with particularly small pore sizes.

I also investigated the data for C1s, O1s and S2p high resolution spectra of the PES membranes (Fig. 3.4). The C1s and O1s high resolution spectra and percentages of each bond type on the PES-g-PAA membrane were consistent with the results of the PVDF-g-PAA membrane.

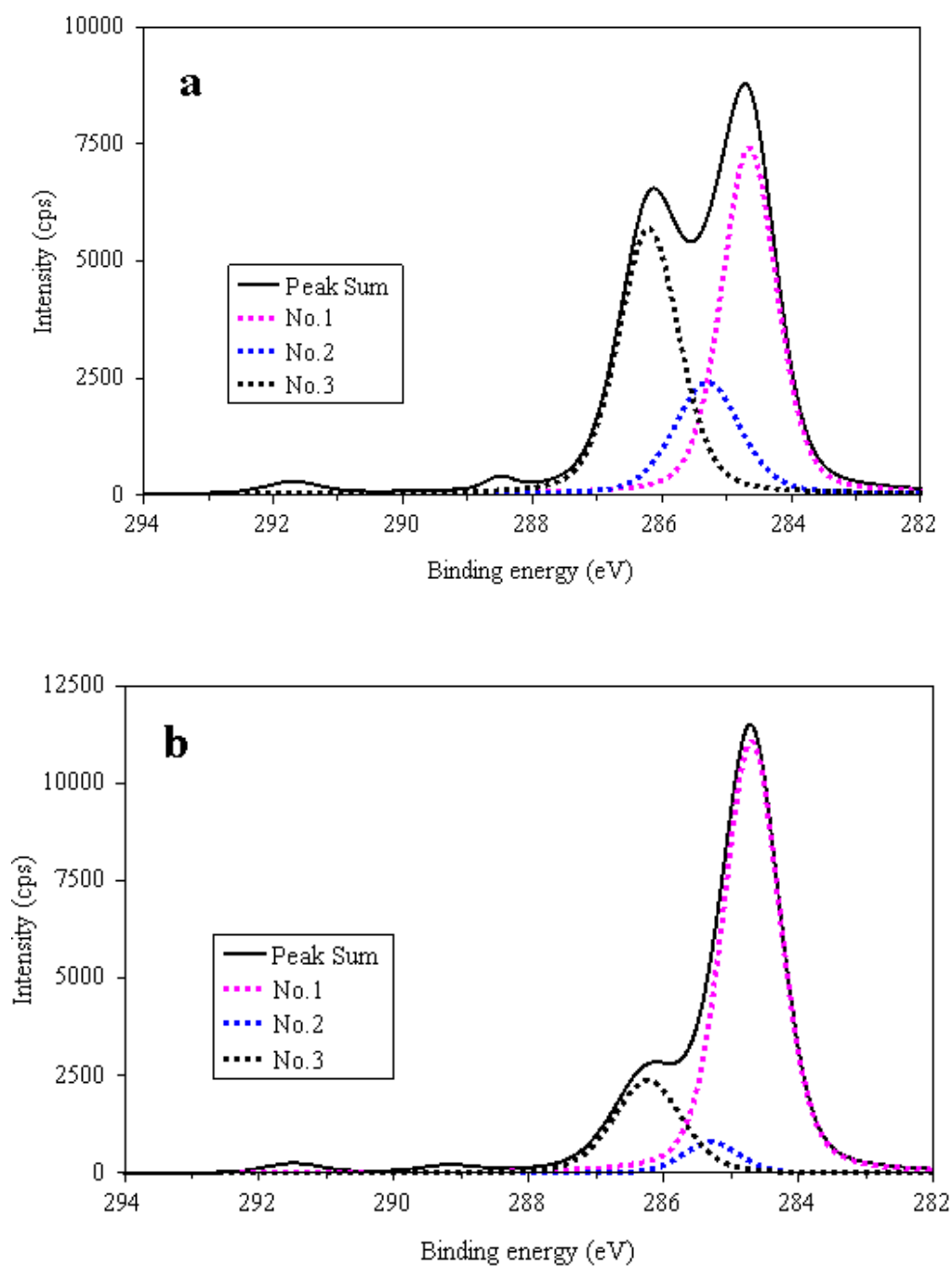


Fig. 3.4. High resolution XPS spectra of C1s. (a) untreated PES membrane and (b) PES membrane treated with argon plasma (treatment: ± 4.0 kVp-p, 180 s).

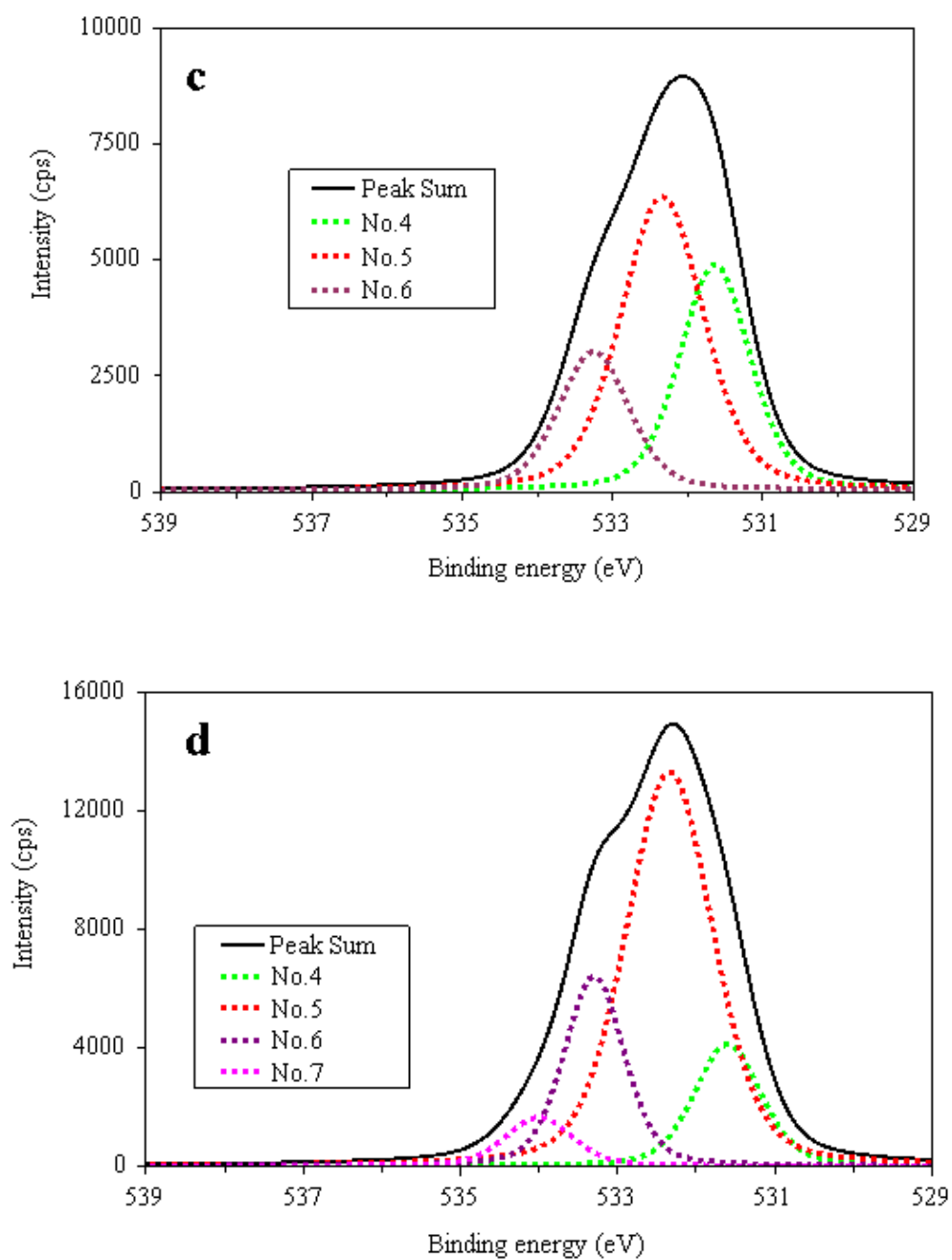


Fig. 3.4. High resolution XPS spectra of O1s. (c) untreated PES membrane and (d) PES membrane treated with argon plasma (treatment: ± 4.0 kVp-p, 180 s).

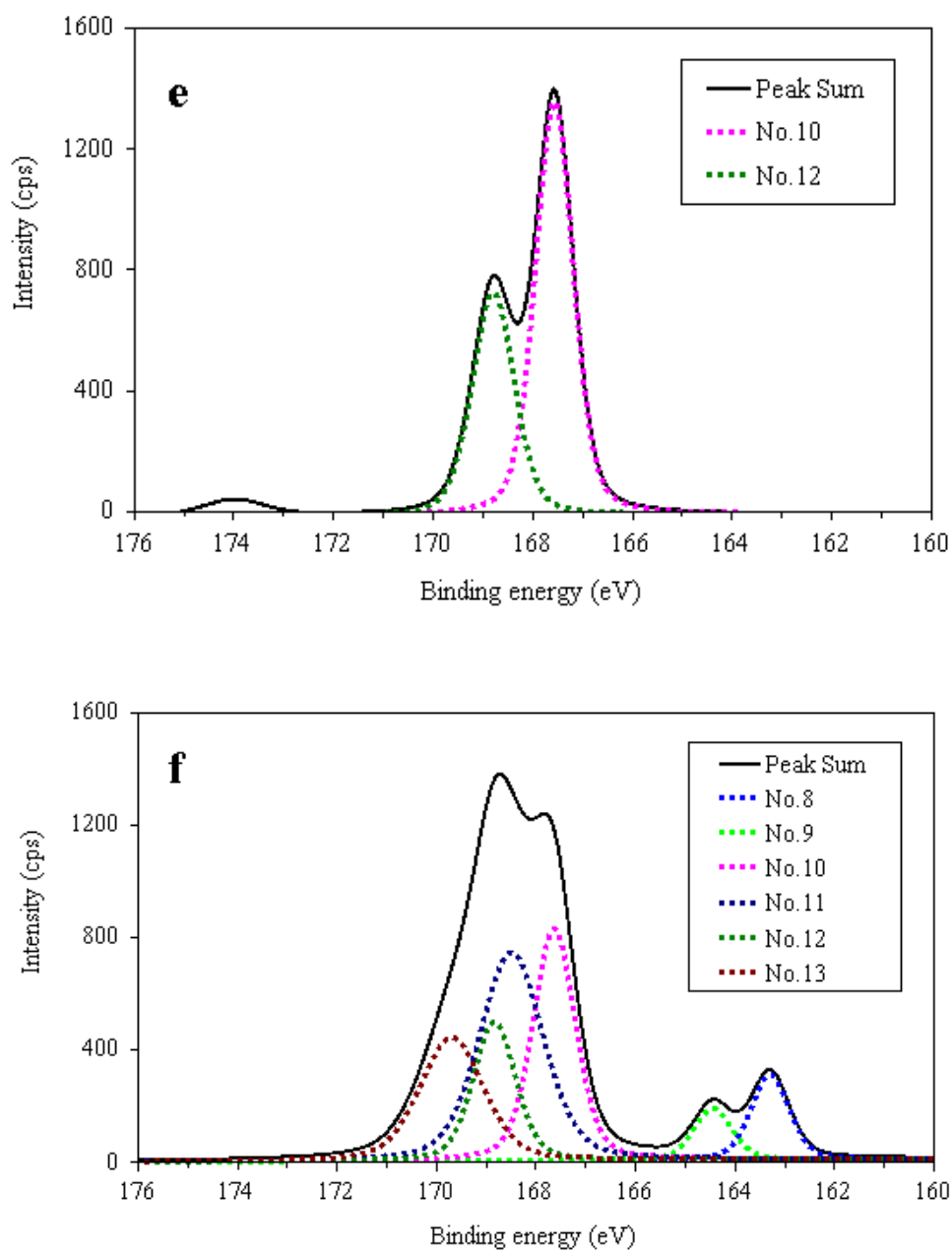


Fig. 3.4. High resolution XPS spectra of S2p. (e) untreated PES membrane and (f) PES membrane treated with argon plasma (treatment: ± 4.0 kVp-p, 180 s).

The C1s high resolution spectrum of the untreated PES membrane was assigned to three peaks at BEs of 284.7 eV due to aromatic $\underline{\text{C}}-\underline{\text{C}}$: No. 1, 285.3 eV due to $\underline{\text{C}}-\text{SO}_2-\underline{\text{C}}$: No. 2 and 286.3 eV due to $\underline{\text{C}}-\text{O}-\underline{\text{C}}$ and phenolic carbons that bond to hydroxy groups : No. 3 (Fig. 3.4a). The $\pi-\pi^*$ shake-up satellite peak was shown at 291.7 eV. The peak area ratio at 286.3 eV (No. 3) was 37%, which was higher than the theoretical value of hydrophobic PES, and the peak area ratio at 284.7 eV (No. 1) was 44%, which was lower than that of hydrophobic PES. These results suggest that the dehydrogenation and oxidation reactions of the benzene ring on the PES membrane progressed, and several phenolic carbons are constituted on the membrane [8]. Secondly, the O1s high resolution spectrum of the untreated PES membrane was deconvoluted into three peaks at BEs of 531.6 eV due to the sulfonyl group, $\text{C}-\underline{\text{SO}}_2-\text{C}$: No. 4, 532.3 eV due to oxygen in the hydroxy group, $\text{R}-\underline{\text{O}}\text{H}$: No. 5 and 533.3 eV due to $\text{C}-\underline{\text{O}}-\text{C}$: No. 6 (Fig. 3.4c). Thirdly, the S2p high resolution spectrum of the untreated PES membrane was deconvoluted into two distinct peaks at BEs of 167.6 eV due to $\text{S}2\text{p}_{3/2}$ for $\text{C}-\underline{\text{SO}}_2-\text{C}$: No. 10 and 168.8 eV due to $\text{S}2\text{p}_{1/2}$ for $\text{C}-\underline{\text{SO}}_2-\text{C}$: No. 12 (Fig. 3.4e).

On the other hand, the C1s high resolution spectrum of the plasma-treated PES membrane was decomposed into three peaks of 284.7 eV due to aromatic $\underline{\text{C}}-\underline{\text{C}}$: No. 1, 285.3 eV due to $\underline{\text{C}}-\text{SO}_2-\underline{\text{C}}$: No. 2 and 286.3 eV due to $\underline{\text{C}}-\text{O}-\underline{\text{C}}$, $\underline{\text{C}}-\text{OH}$ and hydroperoxide ($\text{C}-\underline{\text{C}}\text{H}(-\text{OOH})-\text{C}$) groups: No. 3 (Fig. 3.4b). The peak area ratio of the $\pi-\pi^*$ shake-up was 2%, which was approximately the same level as that of the untreated PES membrane. Secondly, the O1s high resolution spectrum of the plasma-treated PES membrane was curve-fitted with four peaks at BEs of 531.6 eV due to $\text{C}-\underline{\text{SO}}_2-\text{C}$: No. 4, 532.3 eV due to $\text{R}-\underline{\text{O}}\text{H}$: No. 5, 533.3 eV due to $\text{C}-\underline{\text{O}}-\text{C}$ and $\text{C}-\text{CH}(-\underline{\text{O}}\text{OH})-\text{C}$: No. 6, and

534.0 eV for hydroperoxide R-OOH : No. 7 (Fig. 3.4d). Finally, the S2p high resolution spectrum of the plasma-treated PES membrane was deconvoluted into six peaks at BEs of 163.3 eV due to S2p_{3/2} for the sulfide group, C-S-C : No. 8, 164.4 eV due to S2p_{1/2} for C-S-C : No. 9 [28], 167.6 eV due to S2p_{3/2} for C-SO₂-C : No. 10, 168.5 eV due to S2p_{3/2} for the sulfo group, C-SO₃H : No. 11, 168.8 eV due to S2p_{1/2} for C-SO₂-C : No. 12 and 170.1 eV due to S2p_{1/2} for C-SO₃H : No. 13 (Fig. 3.4f).

Based on these results, I proposed an activation mechanism on the membranes treated with atmospheric pressure low-temperature plasma. The each peak area ratio of 285.3 eV (No. 2 in Fig. 3.4b) and 531.6 eV (No. 4 in Fig. 3.4d) was individually 5% and 14%, which was lower than those of the untreated PES membrane. Two deconvoluted peaks were assigned for C-SO₂-C and C-SO₂-C, respectively. These findings suggest that metastable argon, which is the most important active species in the present plasma, collides with the oxygen in the sulfonyl group primarily and results in link cleavage, the formation of radicals such as phenyl radical, and deoxidization reactions. After the oxidation reaction proceeded due to air exposure, it was considered that functional groups were formed such as C-CH(-OOH)-C (No. 7 in Fig. 3.4d) and C-SO₃H (No. 11, 13 in Fig. 3.4f) groups. Furthermore, the peak area ratio of the π - π^* shake-up was comparable before and after plasma treatment. It was also suggested that there was low damage and disruption to the benzene ring by treating with plasma under this condition. Therefore, the phenyl radical and radicals originating from the hydroperoxide groups by thermal treatment would be significantly important initiators to induce graft polymerization with AA on the PES membranes.

3.3.3 Determination of the human IgG adsorption capacity of affinity membranes

Adsorption isotherms of the PVDF/PES-g-PAA-PrA membranes were constructed to investigate the capacity as affinity membranes. Simultaneously, nonspecific adsorption tests were performed with the PVDF/PES-g-PAA membranes prior to immobilization with Protein A. The equilibrium capacities adsorbed on the membranes (q^*) were calculated via the equilibrium concentration of the human IgG dissolved in the liquid (c^*) (Fig. 3.5).

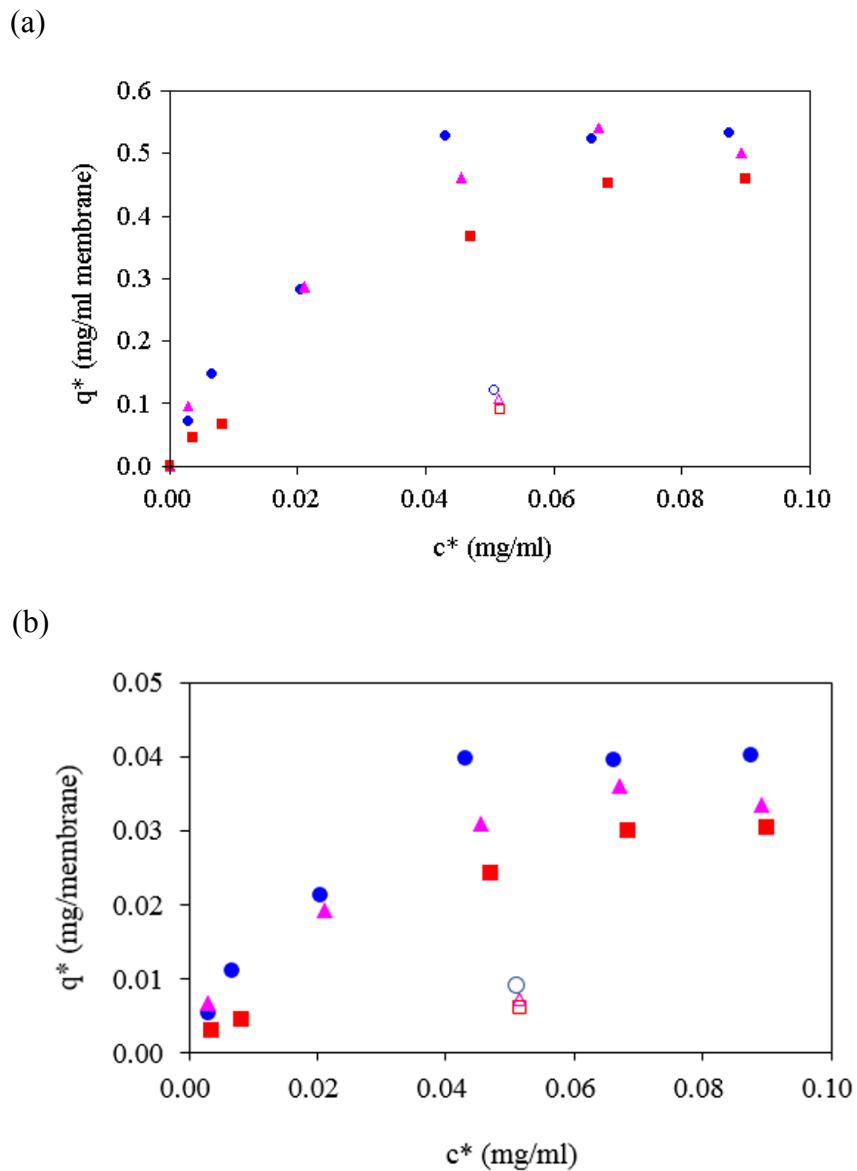


Fig. 3.5. Adsorption isotherms of human IgG binding to the PVDF (pore size 0.45 μ m: closed square, 5.0 μ m: closed triangle) and PES (pore size 0.45 μ m: closed circle) membranes that were immobilized with Protein A. The unit of q^* indicates (a) mg/mL and (b) mg/membrane. Open symbols represent the results of the nonspecific adsorption tests. Adsorption conditions: PBS (-), pH 7.4 as an equilibrium buffer, 20°C, 12 h.

The adsorption isotherms constructed with the PVDF/PES-g-PAA-PrA membranes were fitted with the monolayer Langmuir model. On the other hand, as the result of the nonspecific protein adsorption test, the q^* of the PVDF membranes with pore sizes of 0.45 and 5.0 μm and PES membranes with a pore size 0.45 μm were indicated to have relatively low levels of 0.09, 0.11 and 0.12, respectively. The thermodynamic parameters, which were obtained with the monolayer Langmuir model, are listed in Table 3.3.

Table 3.3

Thermodynamic parameters from adsorption isotherms of human IgG on the PVDF and PES membranes conjugated with Protein A, according to the Langmuir monolayer model. Adsorption conditions: PBS (-), pH7.4 as an equilibrium buffer, 20°C, 12 h. The unit of q^* indicates (a) mg/mL and (b) mg/membrane.

(a)

Membrane	Pore size [μm]	q_m [mg mL ⁻¹]	K_a [L mol ⁻¹]
PVDF-g-PAA-PrA	0.45	0.55	3.3×10^6
	5	0.56	10.6×10^6
PES-g-PAA-PrA	0.45	0.76	4.9×10^6

(b)

Membrane	Pore size [μm]	q_m [mg membrane ⁻¹]
PVDF-g-PAA-PrA	0.45	0.37
	5	0.37
PES-g-PAA-PrA	0.45	0.58

In terms of the PVDF-g-PAA-PrA membranes, it can be seen that the maximum binding capacity (q_m) for a pore size 0.45 μm was 0.55 mg mL^{-1} , which was similar to that with a pore size 5.0 μm . On the other hand, the equilibrium association constant (K_a) for a pore size of 5.0 μm was $10.6 \times 10^6 \text{ L mol}^{-1}$, which was around three times higher than that with a pore size of 0.45 μm . These findings suggest that there is a relationship between the pore size and K_a . Membrane affinity matrices require K_a values above 10^5 L mol^{-1} to ensure efficient adsorption, without risking ligates elution during washing [29]. Compared with capacities of the PVDF/PES-g-PAA-PrA membranes for the same pore size of 0.45 μm , the q_m of the PES membrane was 0.76 mg mL^{-1} , which was 38% higher than that of the PVDF membrane. On the other hand, the K_a of the PES membrane was $4.9 \times 10^6 \text{ L mol}^{-1}$, which was similar to that of the PVDF membrane. To further improve these thermodynamic parameters, it would be meaningful to adopt a cross-linking agent that avoids conjugating with the human IgG binding site of Protein A.

As the latest examples of protein purification adopted similar membranes, Sun and Wu have proposed the BSA separation using mixed matrix membranes (MMMs) comprising of hydroxyapatite (HAP) inside a PES matrix [30]. The BSA adsorption capacity of HAP particles in MMMs reached a maximum (29.4 mg/g membrane) at a pH of 7. Saufi and Fee have demonstrated that the hydrophobic interaction chromatography MMMs, which consisted of a PVDF membrane using a commercial phenyl resin, had static binding capacities (on the membrane volume basis) of 18.4 mg mL^{-1} for β -lactoglobulin [31]. Hence, by integrating affinity membranes and various MMMs that have a distinct separation mode in the downstream processing of the mAb production, the common

issues with packed bed column chromatography, such as complicated packing or operations, could be resolved, leading to reduced production costs and to stable supply for mAbs.

The ligand densities on the PVDF/PES-g-PAA-PrA membranes were measured to investigate the amount of Protein A immobilized on the membrane surface. The results of the stability tests are also included in Table 3.4.

Table 3.4

Ligand density (LD) on the PVDF and PES membranes immobilized with Protein A. Values of ligand densities mean average ($n = 3$). Condition of one cycle: equilibration (PBS (-), pH 7.4, 10 min), adsorption (0.1 mg mL^{-1} human IgG in PBS (-), pH 7.4, 10 min), elution (0.1 mol L^{-1} citric acid buffer, pH 3.0, 10 min), washing (PBS (-), pH 7.4, 10 min) and regeneration (20% (v/v) ethanol, 20 min). The unit of q^* indicates (a) mg/mL and (b) mg/membrane.

(a)

Membrane	Pore size [μm]	Cycle	LD [mg mL^{-1}]	<i>S.D.</i>
PVDF-g-PAA-PrA	0.45	-	0.98	0.07
		5	0.94	0.06
	5	-	1.42	0.10
		5	1.51	0.13
PES-g-PAA-PrA	0.45	-	2.06	0.04
		5	1.98	0.08

(b)

Membrane	Pore size [μm]	Cycle	LD [$\mu\text{g membrane}^{-1}$]	<i>S.D.</i>
PVDF-g-PAA-PrA	0.45	-	16.3	1.1
		5	15.6	1.0
	5	-	23.5	1.7
		5	25.1	2.1
PES-g-PAA-PrA	0.45	-	38.9	0.8
		5	37.4	1.6

Compared with the influence of the PVDF-g-PAA-PrA membranes, the ligand density for a pore size 5.0 μm was 1.42 mg mL^{-1} , which was 49% higher than that for a pore size 0.45 μm . On the other hand, compared with capacities of the PVDF/PES-g-PAA-PrA membranes for the same pore size of 0.45 μm , the ligand density of the PES membrane was 2.06 mg mL^{-1} , which was approximately two times higher than that of the PVDF membrane. One of the explanations is that the O/C atom ratio of the plasma-treated PES membrane was 0.66 (Table 3.2), which was 3.9 times higher than that of the plasma-treated PVDF membranes (Table 3.1). Therefore, it was considered that the functional groups necessary for initiating graft polymerizations were generated more on the plasma-treated PES membranes relative to the PVDF membranes. On the other hand, for the PES membrane, the low accessibility to the ligand with the human IgG is suggested by grafting rich polymerization.

The ligand density was determined using a BCA protein assay as described in the experimental section, and this assay is tuned to detect not only active Protein A but also Protein A that is not capable of binding with human IgG due to the conjugation with the binding site of human IgG. Considering the q_m of the PVDF/PES-g-PAA-PrA membranes for pore size 0.45 μm shown in Table 3.3, the ratio of active Protein A modified on the PVDF-g-PAA-PrA membrane would be higher than that of the PES-g-PAA-PrA membrane.

As a recent related to the study of fabricating functional polymers, Starke *et al.* have introduced a technique for covalent immobilization of trypsin on hydrophilic PVDF and PES membranes both with 0.22 μm pores using electron beam irradiation (150 kGy)

[32]. Comparing the trypsin concentration and activity of these immobilized membranes, the PES membrane showed the higher concentration of $3.48 \mu\text{g cm}^{-2}$ and an activity of $0.49 \text{ nmol min}^{-1}$ in the case of the PVDF membrane ($2.46 \mu\text{g cm}^{-2}$ and $0.36 \text{ nmol min}^{-1}$). However, the enzyme efficiency of trypsin, which was calculated as a quotient of the maximum released substrate per trypsin concentration, turned out to be $5.8 \text{ nmol cm}^2 \mu\text{g}^{-1}$ of the PVDF membrane and was higher than the $3.2 \text{ nmol cm}^2 \mu\text{g}^{-1}$ with the PES membrane described above.

In the results of the stability test, it was confirmed that the ligand densities were comparable, and Protein A was immobilized on the membrane surface rigidly. Castilho *et al.* have reported that the ligand density of poly (vinyl alcohol)-coated membranes, which were the most suitable for IgG purification among the membranes tested in the work, was $4.66 \text{ mg protein A/mL membrane}$ [13]. In summary, it was found that the PVDF/PES-g-PAA-PrA membranes were immobilized with Protein A rigidly, and had the properties of an affinity membrane.

3.3.4 Membrane morphology

It is important to understand whether the microporous structure of the membranes was retained after the plasma treatment and subsequent graft polymerization were conducted. Fig. 3.6 shows the SEM images, obtained with a 3000 \times magnification. Figures 3.6a-3.6c represent the untreated PVDF for pore sizes of 0.45 μm and 5.0 μm , and the PES membrane for a pore size of 0.45 μm , respectively. Figures 3.6d-3.6f show the plasma-treated membranes. The plasma-treated PVDF membrane fibers of the scaffolds for a pore size of 5.0 μm , shown in Fig. 3.6e, maintained the macrovoid formation as well as the untreated PVDF membrane. On the other hand, the plasma-treated PVDF and PES membrane fibers for a pore size of 0.45 μm , shown in Figures 3.6d and 3.6f, had grown slightly thicker than those for each untreated membrane surface. Figures 3.6g-3.6i show the PVDF/PES-g-PAA membranes. The PVDF/PES-g-PAA membranes with a pore size of 0.45 μm were densely modified with PAA. By contrast, the PVDF-g-PAA membrane for a pore size of 5.0 μm definitely retained the macrovoid formation (Fig. 3.6h). These findings clearly indicate that it is effective to apply membranes with a pore size of 5.0 μm to maintain the high porosity and accessibility as affinity membranes.

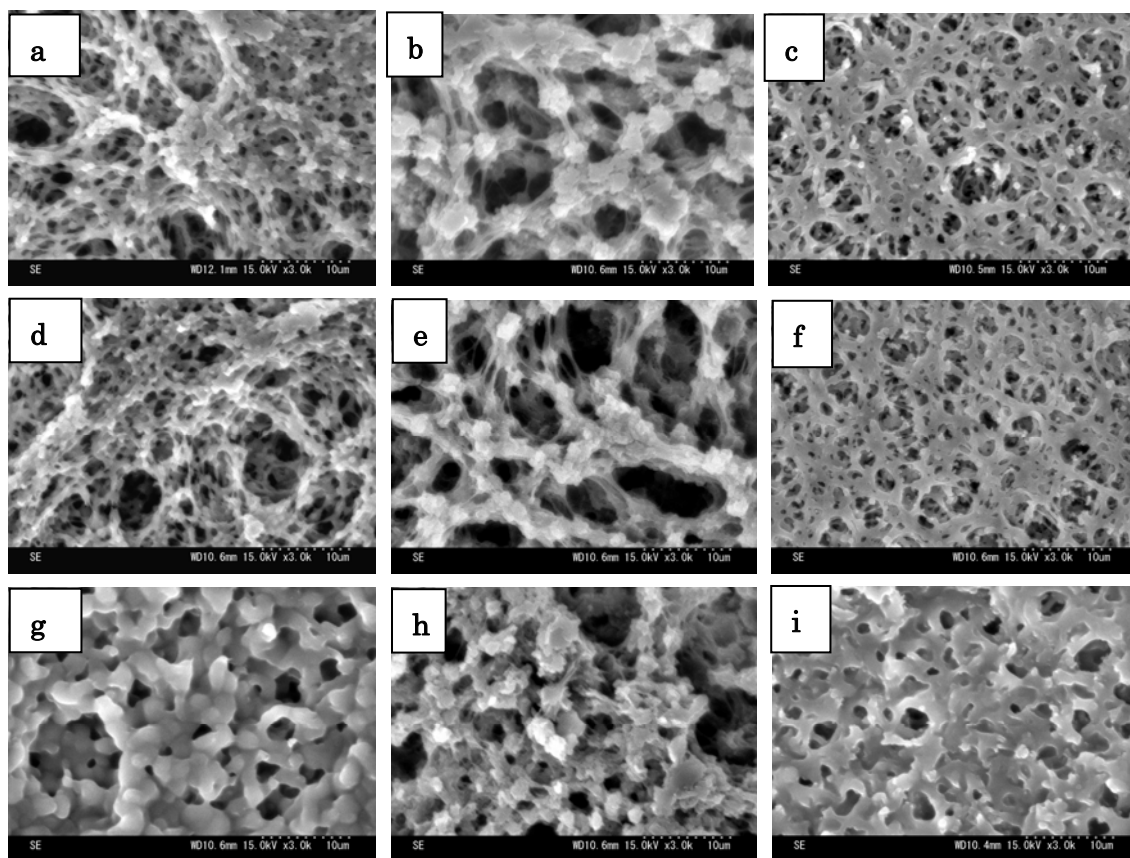


Fig. 3.6. SEM images of PVDF (pore size 0.45 μm (a, d, g) and 5.0 μm (b, e, h)) and PES (c, f, i: pore size 0.45 μm) membrane surfaces. Untreated (a, b, c), treated with argon plasma (d, e, f; treatment: ± 4.0 kVp-p, 180 s) and grafted with AA (g, h, i; treatment: 20% (v/v) AA, 70°C, 20 min). The argon plasma was treated from the above of these membranes.

3.4 Conclusions

I have described the characterization of Protein A-immobilized PVDF and PES membranes. The results of surface property tests on the membranes activated by argon plasma confirmed several functional groups such as hydroperoxide, sulfide and sulfo groups, and I proposed the activation mechanism on polymeric substrates. These findings suggest that the phenyl radical and radicals originating from hydroperoxide groups by thermal treatment are the important precursors to induce graft polymerization with AA on the PES membranes. The porosity of the membrane scaffold was preserved after the plasma treatment. The PVDF membrane for a pore size of 5.0 μm definitely retained the macrovoid formation after the graft polymerization. Protein A was successfully immobilized on the polymer-modified membranes. The adsorption capacities of the Protein A-immobilized membranes were determined and shown to be dependent on the pore size. The ligand density of the Protein A-immobilized PES membranes was approximately two times higher than that of the Protein A-immobilized PVDF membranes. Taken together, I conclude that the atmospheric pressure low-temperature plasma is an excellent tool for activation on the PVDF and PES membranes given the simplicity and effectiveness of this tool, and these polymers are candidates for affinity media for human IgG separation.

Nomenclature

AA Acrylic acid

ATR attenuated total reflection

BCA bicinehoninic acid

EDC 1-(3-Dimethylaminopropyl)-3-ethylcarbodiimide

FT-IR Fourier transform infrared

IgG immunoglobulin G

K_a equilibrium association constant

MES 2 (*N*-morpholino) ethanesulfonic acid

PBS phosphate buffered saline

q_m maximum binding capacity

SEM scanning electron microscopy

Sulfo-NHS *N*-Hydroxysulfosuccinimide

XPS X-ray photoelectron spectroscopy

References

- [1] Dargaville T. R., George G. A., Hill D. J. T.: High energy radiation grafting of fluoropolymers. *Progress in Polymer Science*, 28, 1355-1376 (2003).
- [2] Johns K., Stead G.: Fluoroproducts - the extremophiles. *Journal of Fluorine Chemistry*, 104, 5-18 (2000).
- [3] Liu F., Hashim N. A., Liu Y., Abed M. R. M., Li K.: Progress in the production and modification of PVDF membranes. *Journal of Membrane Science*, 375, 1-27 (2011)
- [4] Kull K. R., Steen M. L., Fisher E. R.: Surface modification with nitrogen-containing plasmas to produce hydrophilic, low-fouling membranes. *Journal of Membrane Science*, 246, 203-215 (2005).
- [5] Zhu L-P., Zhu B-K., Xu L., Feng Y-X., Liu F., Xu Y-Y.: Corona-induced graft polymerization for surface modification of porous polyethersulfone membranes. *Applied Surface Science*, 253, 6052-6059 (2007).
- [6] Rahimpour A.: UV photo-grafting of hydrophilic monomers onto the surface of nano-porous PES membranes for improving surface properties. *Desalination*, 265, 93-101 (2011).
- [7] Steuck M. J.: POROUS MEMBRANE HAVING HYDROPHILIC SURFACE AND PROCESS. 4618533, United States (1986).
- [8] Mezhirova M., Yeh E. B., Sale R.: METHOD FOR PREPARING HYDROPHILIC POLYETHERSULFONE MEMBRANE. 8425814 B2, United States (2013).
- [9] van Reis R., Zydney A.: Bioprocess membrane technology. *Journal of Membrane Science*, 297, 16-50 (2007).

- [10] Nasef M. M., Güven O.: Radiation-grafted copolymers for separation and purification purposes: Status, challenges and future directions. *Progress in Polymer Science*, 37, 1597-1656 (2012).
- [11] Ulbricht M.: Advanced functional polymer membranes. *Polymer*, 47, 2217-2262 (2006).
- [12] Han M. J., Baroña G. N. B., Jung B.: Effect of surface charge on hydrophilically modified poly (vinylidene fluoride) membrane for microfiltration. *Desalination*, 270, 76-83 (2011).
- [13] Castilho L. R., Deckwer W-D., Anspach F. B.: Influence of matrix activation and polymer coating on the purification of human IgG with protein A affinity membranes. *Journal of Membrane Science*, 172, 269-277 (2000).
- [14] Shukla A. A., Hubbard B., Tressel T., Guhan S., Low D.: Downstream processing of monoclonal antibodies - Application of platform approaches. *Journal of Chromatography B*, 848, 28-39 (2007).
- [15] Low D., O'Leary R., Pujar N. S.: Future of antibody purification. *Journal of Chromatography B*, 848, 48-63 (2007).
- [16] Chu P.K., Chen J.Y., Wang L.P., Huang N.: Plasma-surface modification of biomaterials. *Materials Science and Engineering R*, 36, 143-206 (2002).
- [17] Müller M., Oehr C.: Plasma aminofunctionalisation of PVDF microfiltration membranes. *Surface and Coatings Technology*, 116-119, 802-807 (1999).
- [18] Tendero C., Tixier C., Tristant P., Desmaison J., Leprince P.: Atmospheric pressure plasmas: A review. *Spectrochimica Acta Part B*, 61, 2-30 (2006).
- [19] Akashi N., Kuroda S.: Protein immobilization onto poly (vinylidene fluoride) microporous membranes activated by the atmospheric pressure low temperature plasma.

Polymer, 55, 2780-2791 (2014).

[20] Momtaz M., Dewez J.-L., Marchand-Brynaert J.: Chemical reactivity assay and surface characterization of a poly(vinylidene fluoride) microfiltration membrane (“Durapore DVPP”). *Journal of Membrane Science*, 250, 29-37 (2005).

[21] Persson K. M., Capannelli G., Bottino A., Trägårdh G.: Porosity and protein adsorption of four polymeric microfiltration membranes. *Journal of Membrane Science*, 76, 61-71 (1993).

[22] Langmuir I.: The adsorption of gases on plane surfaces of glass, mica and platinum. *Journal of the American Chemical Society*, 40, 1361-1403 (1918).

[23] Castilho L. R., Anspach F. B., Deckwer W-D.: Comparison of affinity membranes for the purification of immunoglobulins. *Journal of Membrane Science*, 207, 253-264 (2002).

[24] Huse K., Böhme H.-J., Scholz G. H.: Purification of antibodies by affinity chromatography. *Journal of Biochemical and Biophysical Methods*, 51, 217-231 (2002).

[25] Hidzir N. M., Hill D. J. T., Taran E., Martin D., Grøndahl L.: Argon plasma treatment-induced grafting of acrylic acid onto expanded poly(tetrafluoroethylene) membranes. *Polymer*, 54, 6536-6546 (2013).

[26] Lee Y. M., Shim J. K.: Plasma Surface Graft of Acrylic Acid onto a Porous Poly(vinylidene fluoride) Membrane and Its Riboflavin Permeation. *Journal of Applied Polymer Science*, 61, 1245–1250 (1996).

[27] Huang F. L., Wang Q. Q., Wei Q. F., Gao W. D., Shou H. Y., Jiang S. D.: Dynamic wettability and contact angles of poly(vinylidene fluoride) nanofiber membranes grafted with acrylic acid. *Express Polymer Letters*, 4, 551–558 (2010).

[28] Wavhal D. S., Fisher E. R.: Hydrophilic modification of polyethersulfone

membranes by low temperature plasma-induced graft polymerization. *Journal of Membrane Science*, 209, 255-269 (2002).

[29] Beeskow T. C., Kusharyoto W., Anspach F. B., Kroner K. H., Deckwer W.-D.: Surface modification of microporous polyamide membranes with hydroxyethylcellulose and their application as affinity membranes. *Journal of Chromatography A*, 715, 49-65 (1995).

[30] Sun J., Wu L.: Polyether sulfone/hydroxyapatite mixed matrix membranes for protein purification. *Applied Surface Science*, 308, 155–160 (2014).

[31] Saufi S. M., Fee C. J.: Mixed matrix membrane chromatography based on hydrophobic interaction for whey protein fractionation. *Journal of Membrane Science*, 444, 157–163 (2013).

[32] Starke S., Went M., Prager A., Schulze A.: A novel electron beam-based method for the immobilization of trypsin on poly(ethersulfone) and poly(vinylidene fluoride) membranes. *Reactive & Functional Polymers*, 73, 698–702 (2013).

Chapter 4 Summary

The final goal of this study was to prepare and characterize of Protein A-immobilized PVDF and PES membranes. As the method of mild surface modification, the atmospheric pressure low temperature plasma was adopted prior to the immobilization.

The first goal of this study was to reveal the activation mechanism on the membranes activated by the plasma and immobilize BSA as a model protein. The optimum conditions for the plasma treatment, graft polymerization and immobilization were determined in order to minimize the deterioration of the PVDF membrane and establish the high reproducibility. The plasma-treated PVDF membrane was studied chemically by measuring the high resolution XPS spectra in order to reveal the functional groups generated by the optimum plasma treatment. As the result of that, it was found that the hydroperoxide group played an important role for initiating the graft polymerization. As the results of studying the membranes morphologies, the porosity of the membrane scaffold was preserved after the plasma treatment. These findings were described in the chapter 2.

The second goal of this study was to characterize the properties of Protein A-immobilized the membranes prepared by the optimum condition. The activation mechanism of the plasma-treated PES membrane was also proposed. Protein A was successfully immobilized on the polymer-modified PVDF and PES membranes. The adsorption capacities with human IgG were confirmed according to the monolayer

Langmuir model, and the ligand densities were also determined. As the results of that, ligand density of the Protein A-immobilized PES membranes was approximately two times higher than that of the Protein A-immobilized PVDF membranes. These results were described in the chapter 3.

In summary, it was concluded that the atmospheric pressure low temperature plasma is an excellent tool for activating on the PVDF and PES membranes, and PVDF and PES polymers are candidates as affinity media for human IgG separation.

List of publications

Related articles

[1] Naohisa Akashi and Shin-ichi Kuroda.: Protein immobilization onto poly (vinylidene fluoride) microporous membranes activated by the atmospheric pressure low temperature plasma, *Polymer*, 55, 2780-2791 (2014).

[2] Naohisa Akashi and Shin-ichi Kuroda.: Preparation and characterization of Protein A-immobilized PVDF and PES membranes, *eXPRESS Polymer Letters*, in press.

Reference articles

[1] Naohisa Akashi, Katsuhiko Hosoi, Shin-ichi Kuroda.: Studies on the surface of PTFE membranes treated with atmospheric pressure low temperature plasma of Ar and Ar/H₂, *Advanced Materials Research*, in press.

Acknowledgements

First of all, I would like to thank professor Shin-ichi Kuroda. I really appreciate all his contributions of time, idea and support. He advised me for physicochemical interpretations of my experimental data. I am thankful for assistant professor Takahiko Kawai. He taught me operations of the atomic force microscope. I am thankful for associate professor Shoji Takigami who belongs in Center for Material Research by Instrumental Analysis of Gunma University. He permitted me to use X-ray photoelectron spectroscope, Fourier transform infrared spectroscope and scanning electron microscope kindly. I am thankful for professor Yutaka Kawahara and associate professors Hiroyuki Oku, Masaru Yoneyama and Shoji Takigami. They gave me some advices to improve the presentation of the doctoral dissertation.

I appreciate for the all members of the Kuroda group, and thankful for Ph.D. Katsuhiko Hosoi. He taught me operations of some experimental devices. I am thankful for graduates, Ph.D. Norihito Mizote and Mr. Yuta Watanabe. They taught me operations of XPS kindly. I am thankful for a graduate, Ph.D. Vinita Sharma. She cooperated with checking my 1st research paper for grammatically. I am thankful for a graduate, Mr. Yujiro Tanaka. He prepared some equipment for me soon after I entered graduate school. I am thankful for Merck Millipore Company and other suppliers. They provided me experimental materials in a timely manner. I am thankful for Kyowa Hakko Kirin Co.,Ltd. The company supported and gave me an opportunity to study in this field. Lastly, I would like to thank my wife for all encouragement.